Draft
Pending technical review

PAVEMENT SUBGRADE PERFORMANCE STUDY

Test Section 711

Subgrade AASHTO soil type A-7-5 at 25 percent gravimetric moisture content

by

Edel R. Cortez [1]

Subgrade Moisture Content	AASHTO Soil Type			
	A-2-4	A-4	A-6	A-7-5
M1	Optimum 10 % TS 701	Optimum 17 % TS 702	Optimum 16 % TS 709	Optimum 20.5 % TS 712
M2	12 % TS 707	19 % TS 704	**19 %** **TS 708**	**21 %** **TS 710**
M3	15 % TS 703	23 % TS 705	22% TS 706	25 % TS 711

[1.] U.S. Army Cold Regions Research and Engineering Laboratory, 72 Lyme Road,
Hanover, New Hampshire 03755, United States

EXECUTIVE SUMMARY

This report is one of a series of reports on the national pooled-fund research project titled Subgrade Performance Study (SPR-208). The hypothesis for this study is that the failure criterion depends on the subgrade soil type and the in-situ moisture content. Current mechanistic design procedures incorporate the results from the AASHO Road Tests conducted in the late nineteen fifties. However, the AASHO Road Tests were all conducted on only one soil type (AASHTO type A-6). The tests results reflect the combined effects of traffic loads and seasonal variations. Applying failure criteria based on the AASHO Road Tests to other soil types, at different moisture contents and different climate introduces significant uncertainty.

In recent decades much progress has been achieved in computer and sensor technologies. Reliable measurements of in-situ stress and strain are now feasible and practical. These technological advances enable the development of more reliable pavement failure criteria that consider the effects of subgrade soil type and moisture condition.

Transportations agencies from nineteen US states are contributing to a research initiative that will develop the bases for new pavement failure criteria that is adequate for the most common subgrade soil types found in the United State at various soil moisture contents. As part of the research program, four subgrade soils were selected for testing. Twelve full-scale pavement test sections were built in the Frost Effects Research Facility (FERF) at the U.S. Army Cold Regions Research and Engineering Laboratory (CRREL). The test sections were practically identical, except for the subgrade soil type and the moisture condition. Three test sections were built with each subgrade soil type. One of these test sections contained the subgrade soil at optimum moisture condition. The other two test sections contained the same subgrade soil type at two different levels of moisture content above optimum. The test sections consisted of 75 mm of asphalt concrete, 229 mm of crushed base and 3 m of the test subgrade soil type at a pre-determined moisture content. The current test section was named Test Section 711. The subgrade soil was classified as AASHTO type A-7-5, equivalent to a soil type MH in the Unified Soil Classification System. Although the target moisture content was 26 percent, the actual as-built average subgrade soil gravimetric moisture content was 25 percent. According to laboratory modified Proctor tests for this soil, the optimum moisture content was 20.5 percent and the maximum density was 1700 kg/m^3 (106.1 lb/ft^3).

Accelerated traffic was applied by means of a Heavy Vehicle Simulator (HVS). The traffic axial load was varied for each test window, ranging from 53.4 to 195.6 kN (12 to 44 kips). The load was applied through a dual truck tire assembly representing a half axle of a standard truck. Therefore, a 40-kN (9-kip) semi-axial load is equivalent to an 80 kN (18-kip) load applied with a complete truck axle. The tire pressures were kept at 689 kPa (100 psi).

The test section was built inside the FERF where subgrade soil moisture and temperature conditions were controlled and kept constant. The test section contained six test windows. Each effective test window was approximately 6.0 m long and 0.91 m wide. Additional length was provided at each end for acceleration and deceleration of the tire assembly. Loading was applied unidirectionally at an average speed of 12 km/hr. The test windows were subjected to approximately 600 load repetitions per hour. The HVS applied traffic 23 hours per day. The remaining hour was used for maintenance.

Stress, strain, and surface rut measurements were taken at various stages throughout the traffic testing. Stress and strain sensors were located at various depths in the base course

and the subgrade. Permanent strain (while no traffic was occurring) and resilient strain (during the passing of the tire assembly) were measured at continuous layers from the asphalt surface down to a depth of 1.52 m. This configuration provided a means to define a distribution of deformations and calculation of average strain for each layer. Adding the layer deformations and comparing to the rut depth measured at the pavement surface provided a way to calibrate the subsurface deformation measurements. Surface rutting was measured with a laser profilometer.

This report contains a description of the test section, construction, instrumentation, pavement response to traffic loads, and pavement performance.

INTRODUCTION

As part of an international study on pavement subgrade performance, several full-scale test sections were constructed in the Frost Effects Research Facility (FERF) at the Cold Regions Research and Engineering Laboratory (CRREL) in Hanover, New Hampshire. CRREL is a component of the Engineers Research and Development Center (ERDC) which is the research and development division of the US Army Corps of Engineers. The tests were conducted indoors at approximately 20°C (68°F). They were instrumented with stress cells, strain gages, moisture gages, and temperature sensors. The test sections were subjected to accelerated loading using CRREL's Heavy Vehicle Simulator (HVS). Pavement failure was defined at 12.5 mm (0.5 in.) surface rut depth, or the development of asphalt cracks 9.5 mm (3/8 in.) wide. Surface rut depth measurements were taken periodically during the accelerated load tests. At the same time, subsurface stress and strain measurements were also taken. A detailed overview of the project can be found in Janoo et al (2001). The test sections consisted of a 76-mm (3 in.) asphalt concrete (AC) layer, a 229-mm (9 in.) crushed gravel base and 3 m (10 ft) of subgrade soil. All the test sections in this research project were alike in geometry, instrumentation, and materials, except for the subgrade soil type and moisture content. The test sections were constructed using several subgrade soil types conditioned at various moisture contents. For each test section, provisions were made to maintain the temperature and moisture content as constant as possible. The test matrix for this study is shown in the table below.

Table 1. Experimental test matrix.

Subgrade Moisture Content	AASHTO Soil Type			
	A-2-4	A-4	A-6	A-7-5
M1	Optimum 10 % TS 701	Optimum 17 % TS 702	Optimum 16 % TS 709	Optimum 20.5% TS 712
M2	12 % TS 707	19 % TS 704	**19 %** **TS 708**	**21%** **TS 710** **Borderline soil A-6 and A-7-6**
M3	15 % TS 703	23 % TS 705	22% TS 706	25% TS 711

This reports deals with the construction, accelerated traffic testing, and pavement response of Test Section 711. As shown in Table 1, the subgrade soil in this test section was classified as AASHTO soil type A-7-5. The subgrade gravimetric moisture content was 25 percent. The laboratory CBR test results indicate that, at this moisture content, the subgrade soil had a CBR of 13 percent.

DESCRIPTION OF THE TEST SECTION

The pavement structure consisted of a 76-mm (3-in) hot mixed asphalt (HMA) layer, a 229-mm (9-in) crushed gravel base course, and 3 m (10 ft) of subgrade soil.

The test section was divided into six test windows. A test window is an area where traffic is applied. An effective test window was 0.91 m (3 ft) wide by 6.08 m (20 ft.) long, excluding acceleration and deceleration areas. The thickness and material properties for all test windows were designed to be constant, but the traffic load intensity was designed to vary from one test section to another.

Each test window was instrumented with embedded sensors to measure in-situ stress, strain, moisture and temperature at various locations within the pavement structure. Dynatest® stress cells were used to measure stress in the subgrade soil. Geokon® stress cells were embedded in the unbound base course. εmu coils were installed in three stacks able to measure displacement between coil pairs in vertical, longitudinal and transverse directions. Vertical displacements were measured in ten layers to a depth of approximately 1.52 m (5 feet). Strains were calculated from the displacement measurements. Campbell Scientific® CS615 sensors were used to record volumetric soil moisture content in the base course and subgrade during the accelerated traffic period. Additionally, strings of thermocouples were used to record subgrade, base, asphalt and air temperatures.

The test section was built indoors where the temperature and soil moisture were controlled, and kept practically constant during the test period. The test basin where the test section was built consisted of 3 lateral concrete walls, an access ramp also made of Portland cement concrete, and a concrete floor. During construction, much care was applied to retain the soil moisture by temporarily covering the top soil layer with tarps. Later, the asphalt layer helped to contain the subgrade and base course moisture.

Ordinary construction equipment was used to build the test sections, but the quality control and quality assurance testing were more rigorous than those commonly used in regular construction.

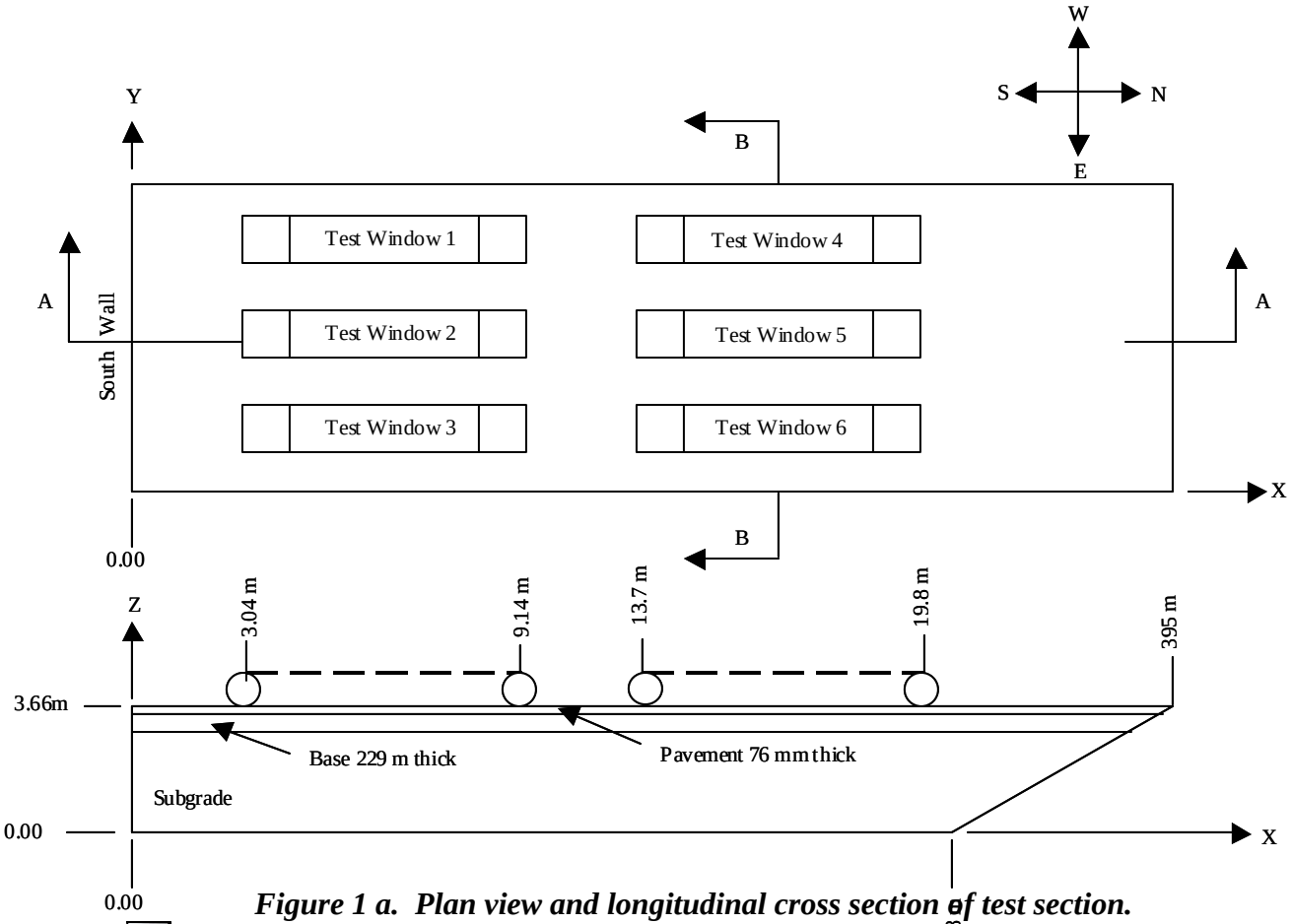

Figure 1 a. Plan view and longitudinal cross section of test section.

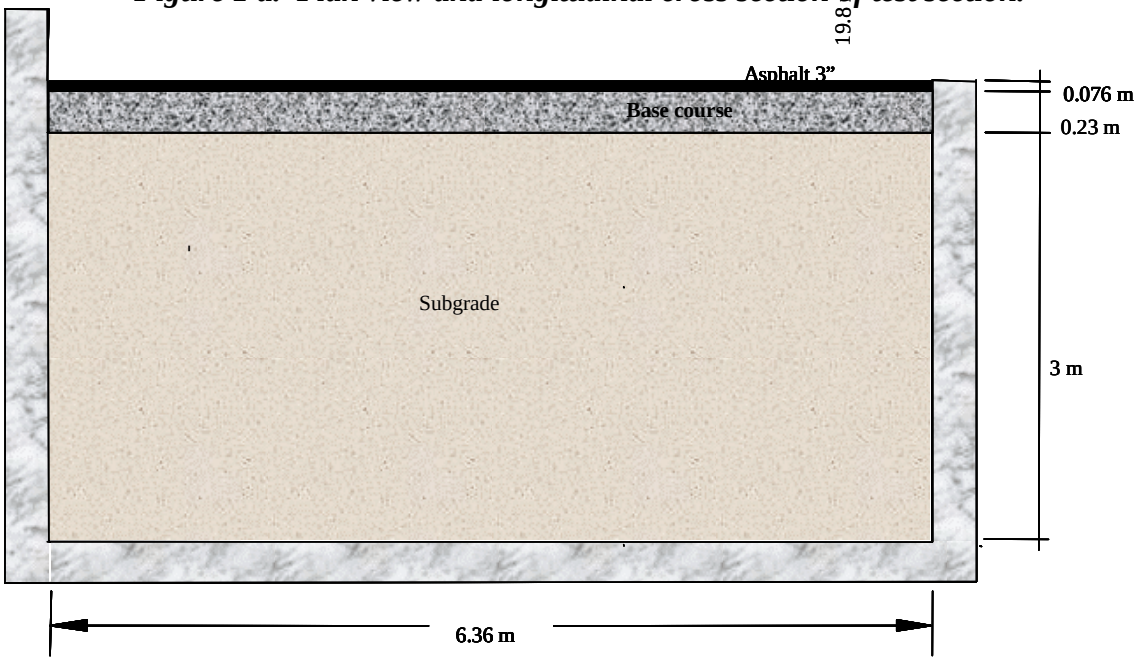

Figure 1 b. Transversal cross section.

MATERIAL PROPERTIES

Laboratory tests were conducted on representative samples of the subgrade soil and the base course soil. The battery of tests included modified proctor, laboratory CBR, Atterberg limits, sieve analysis, hydrometer, and specific gravity tests.

Figure 1 shows grain size distributions for the subgrade soil and for the base course soil. The subgrade soil has approximately 88 percent passing the 0.074-mm (#200) sieve and 33 percent finer than 0.002 mm (clay content). The average liquid limit (LL) and plasticity index (PI) of the soil were 55 percent and 20 percent respectively. According to the American Association of Highway and Transportation Officials (AASHTO) soil classification system, this soil falls within the A-7-5 region, but near the boundary of the A-7-6 region. According to the Unified Soil Classification System, the subgrade soil was a MH soil (High liquid limit silt). The average specific gravity of the subgrade soil was 2.71.

The base course material was made of unbound crushed stone. It was classified as an AASHTO type A-1 soil. According to the Unified Soil Classification System, the base course soil was type GP-GM (mix of poorly graded gravel and silty gravel). About 11 percent by weight of the base course soil particles passed through the sieve 0.074-mm (#200) sieve. The fines were classified as non-plastic.

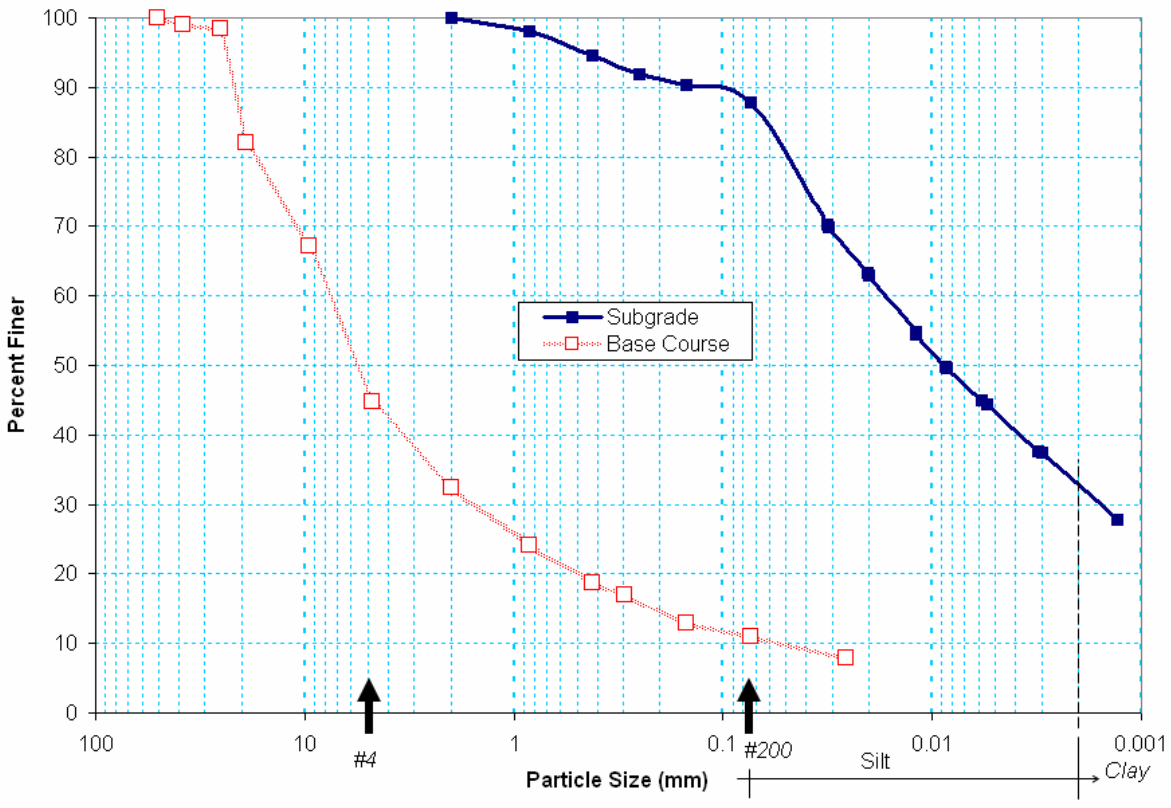

Figure 2. Grain size distribution for the subgrade soil and base course soils.

The maximum density and optimum gravimetric moisture content for the subgrade soil were 1700 kg/m^3 (106.1 pcf) and 20.5 percent respectively. The design moisture content for this test section was 26 percent, but the average as-built subgrade moisture content was 25 percent. The laboratory CBR for this moisture content was approximately 13 percent.

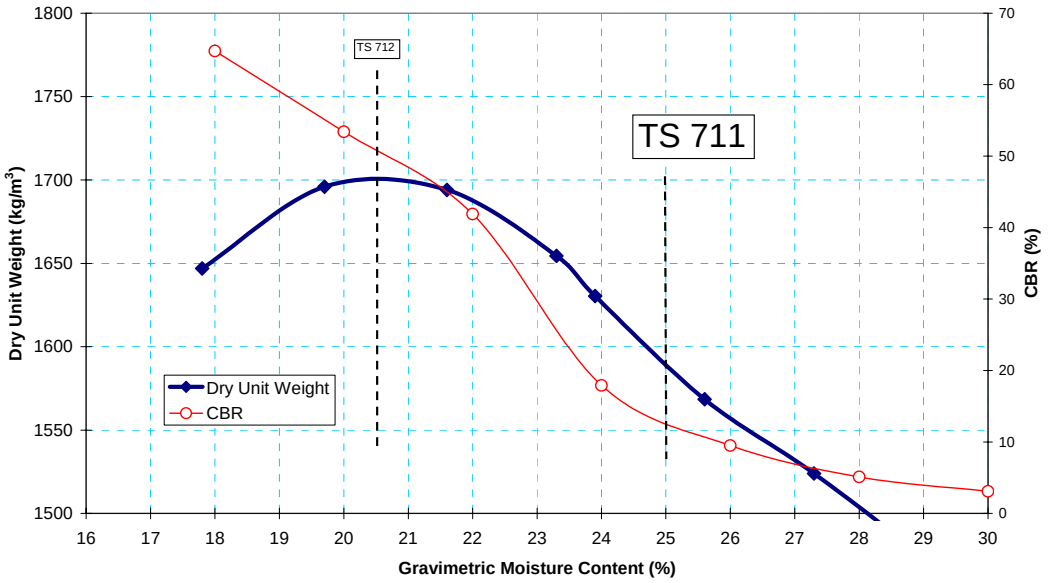

Figure 3. Subgrade modified Proctor and laboratory CBR test results.

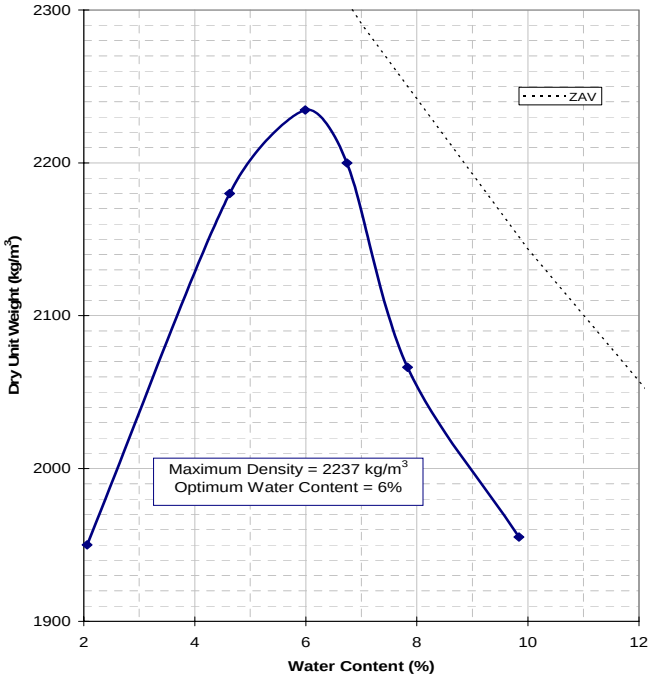

Figure 4. Base course modified Proctor test results.

The modified Proctor test results shown in Figure 4 indicate that the optimum gravimetric moisture content of the base course material was 6 percent and the maximum density was 2237 kg/m^3 (139.5 pcf). Obtaining this moisture content with high hydraulic conductivity materials is difficult in practice. The average moisture content of the base course material during construction was 5.9 percent.

Table 2. Summary of properties of the subgrade soil used in Test Section 711.

AASHTO	A-7-5
USCS	MH
Spec. Gravity	2.72
LL (%)	55
PI	21
Optimum Moisture Content (%)	20.5
Maximum Density (kg/m^3)	1590
% passing #10	100
% passing #200	88
% finer than 0.002 mm	33

The asphalt concrete material of the binder course conformed to the Vermont Type II standard, with 19-mm maximum aggregate particle size and 4.5% of asphalt binder PG-58-34. The asphalt concrete material of the wearing course conformed to the Vermont Type III standard, with 13-mm maximum aggregate particle size and 5.3% of asphalt binder PG-58-34. The nominal thickness of the binder course was 51 mm. The nominal thickness of the wearing course was 25 mm.

CONSTRUCTION OF THE TEST SECTION

The subgrade was built in layers 150-mm (6-in.) thick. The soil was first placed at a moisture condition lower than the target moisture content. The soil was rototilled and water was gradually added until the target soil moisture content was reached. Then, the soil was compacted with 8 passes of a 10-Ton (9,072-kg) steel roller in static mode, followed by 4 passes in vibratory mode. Moisture and density quality control measurements were taken using a nuclear gauge. Additional roller compacting was applied to any low density region until the density was at least 95 percent of the modified proctor density for the given moisture content.

The base course was placed in 2 layers 114.3-mm (4.5-in.) thick for a total of 228.6 mm (9 inches). Finally, the AC layer was placed in two lifts for a total of 76 mm (3 inches).

CONSTRUCTION QUALITY CONTROL

During the construction of the subgrade, a series of tests were conducted on each of the compacted layers. Measurements included layer thickness taken with a survey level, and moisture-density measurements taken with a nuclear gauge. Falling weight deflectometer (FWD) tests were conducted on top of the asphalt concrete prior to traffic testing.

The mean moisture content of the subgrade was 25.1 percent. The average moisture content of the base course during construction was 5.9 percent.

The mean dry density of the subgrade was 1539 kg/m^3 (96.1 pcf). The mean dry density of the base course was 2350 kg/m ^{3} (146.7 pcf). The mean density of the AC was 2300 kg/m^3 (143.6 pcf).

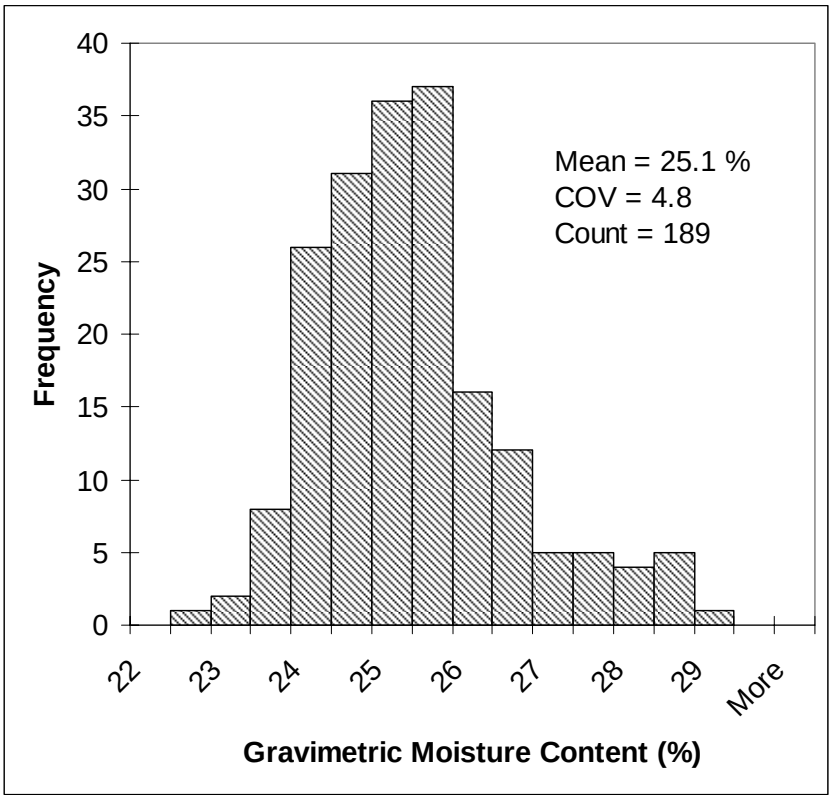

Figure 5. Subgrade moisture content.

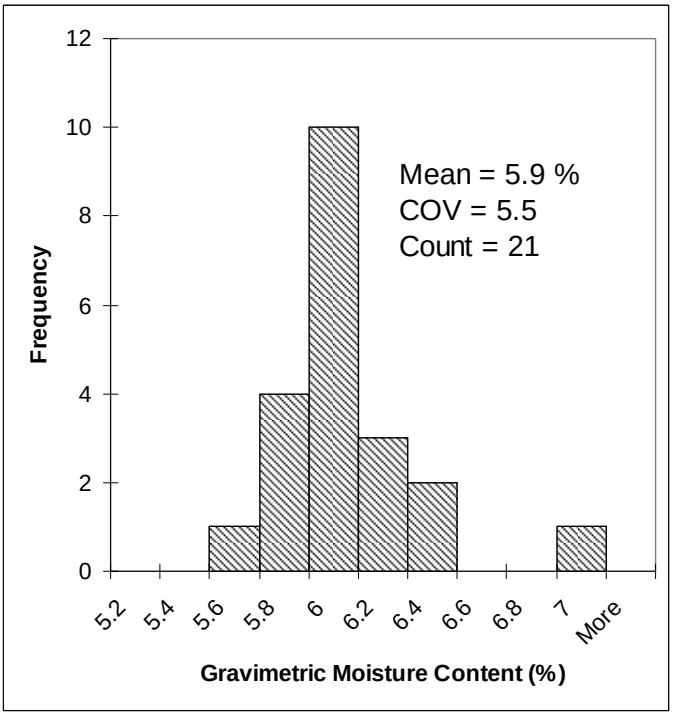

Figure 6. Base course gravimetric moisture content.

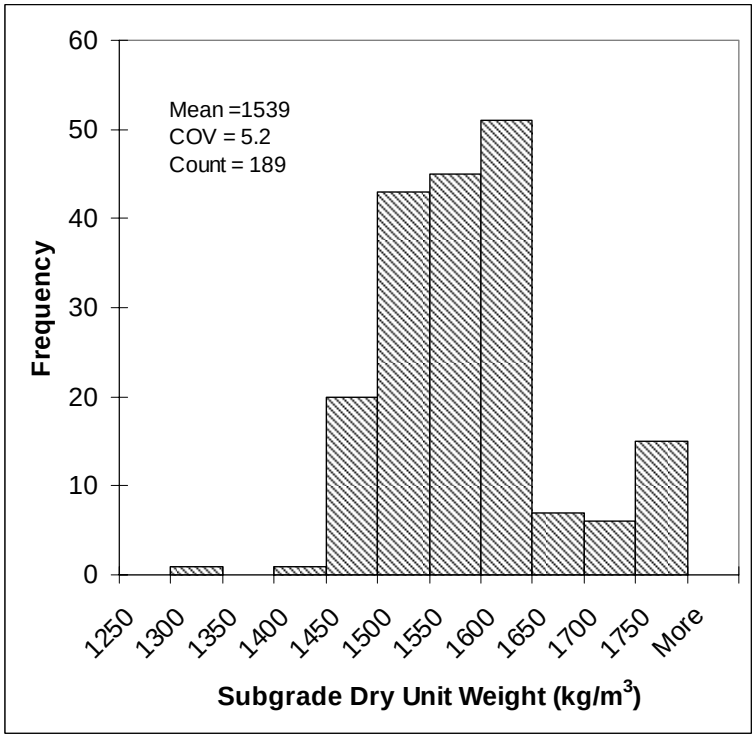

Figure 7. Subgrade dry unit weight.

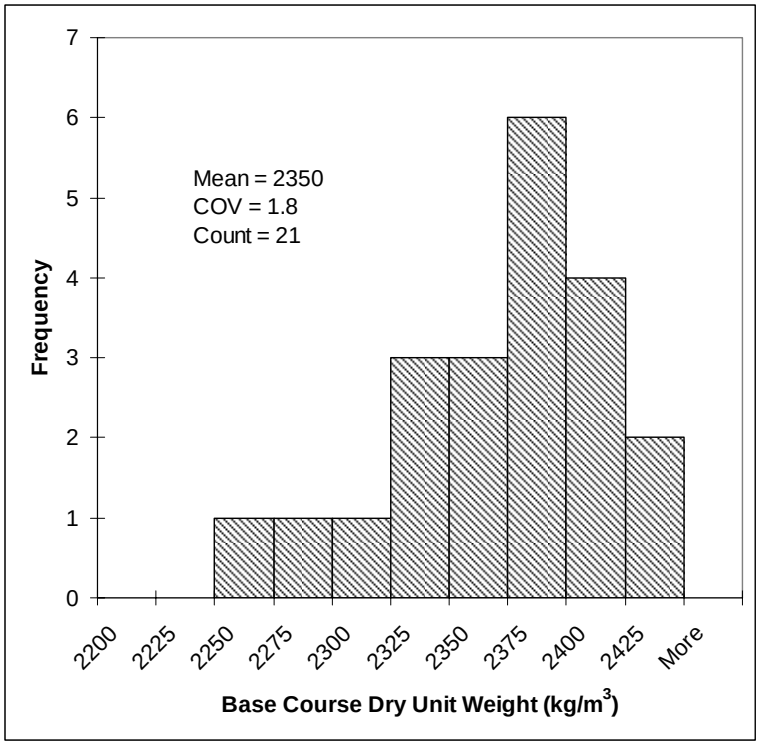

Figure 8. Base course dry unit weight.

INSTRUMENTATION

Instrumentation for measuring stress, strain, temperature, and moisture content were installed in the pavement structure during construction of the test section. More details about the instrumentation can be found in Janoo et al., 2002. The locations of the gages in the test section were similar to those in previous test sections.

Displacement measurements were made in the base and subgrade by means of εmu coils. Strain can be deducted from displacement measurements between coil pairs in either coaxial or co-planar arrangements. The sensors were placed 150 mm center to center. Displacements were measured in the longitudinal (x), transversal to traffic (y), and vertical (z) direction of loading. Displacements in the vertical direction were measured in a series of layers down to a depth of 1.52 m.

Figure 9. Emu coils in a co-planar arrangement to measure longitudinal and transversal displacements. ***A US 25-cent coin is included for scale reference.***

A triaxial Dynatest® stress cell set was installed at a depth of 76 mm (3 in.) below the top of the subgrade in all test windows. In Test Window 2 an additional triaxial stress cell set was installed at a depth of 381 mm (15 in.) below the top of the subgrade. The diameter of the Dynatest® stress cells was 76 mm (3 in.).

Geokon® stress cells were installed in the middle thickness of the base course in each of Test Windows 2 and 5 in triaxial sets. In Test Window 6, Geokon stress cells were installed to measure only vertical stress at depths 51 mm (2 in.) below the bottom of the asphalt, at 25.4 mm (1 in.) above the base course-subgrade interface, and 127 mm (5 in.) below the top of the subgrade.

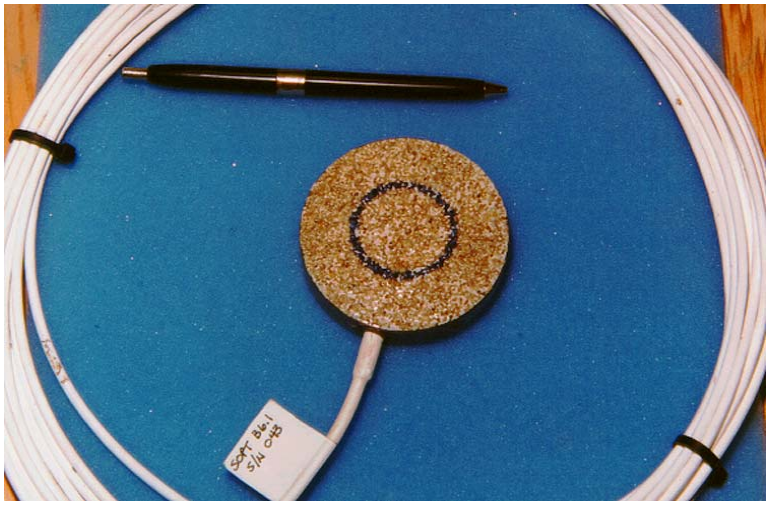

Figure 10. Dynatest® stress cell used in the subgrade.

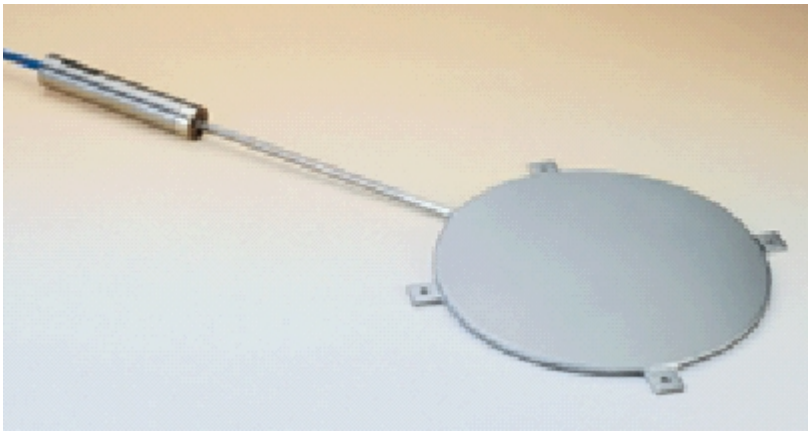

Figure 11. Geokon® stress cell used in the base course and subgrade.

Campbell Scientific® reflectometer soil moisture probes model CS615 were used to measure the moisture content in the base and subgrade during the traffic tests. These sensors measure the oscillation frequency between two rods embedded in the moist soil. The oscillation frequency is related to the dielectric constant that changes with moisture content, and, to a lesser degree, with temperature. The sensor readings are also affected by salinity, mineralogy and presence of organic materials. Volumetric moisture content is converted to gravimetric moisture content through weight-volume relationships and soil specific gravity. These sensors alone are not accurate enough for the purpose of this study, but this deficiency was corrected by oven dry measurements during construction and during the forensic evaluation.

Moisture sensors were located at three depths at each of three horizontal locations. There were moisture sensors in the middle of the base course, and in the subgrade at 15 cm (6 in.) and 61 cm (2 ft.) below the top of the subgrade.

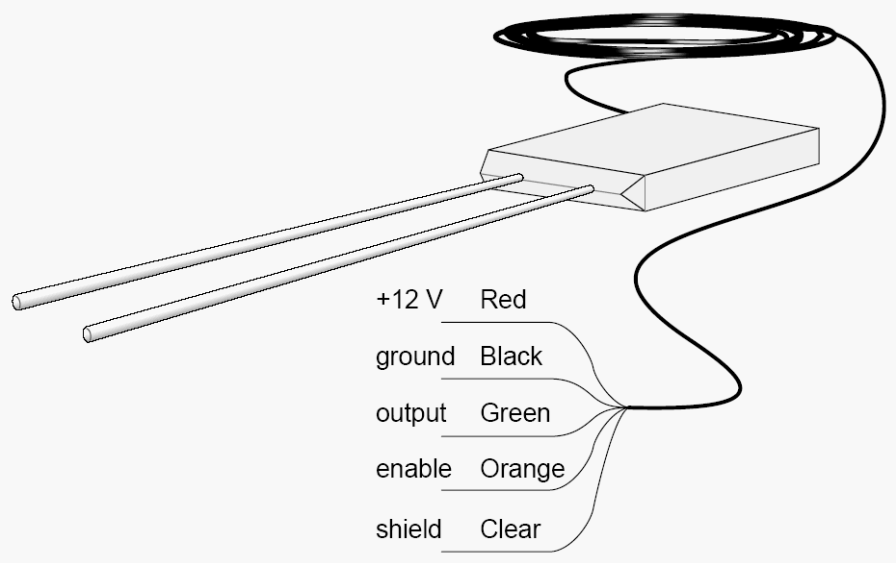

Figure 12. Campbell Scientific® reflectometer soil moisture probes model CS615.

Subsurface temperatures were taken using thermocouple sensors. The thermocouples have an accuracy of ± 0.5°C. The subsurface temperature sensors were installed at three horizontal locations within the test section in the asphalt concrete, base course and at two depths into the subgrade. Air temperatures were also measured.

TRAFFIC TESTING

The test windows were subjected to accelerated traffic loads using CRREL's Heavy Vehicle Simulator (HVS).

The following tests were conducted:

1. Prior to the accelerated load tests, FWD measurements were conducted on the surface of the AC layer at locations in a representative grid arrangement.
2. Initial transverse profiles of each test window were measured using a laser profilometer. The laser source and sensor were located 45 cm (1.5 ft.) above the pavement surface. Each cross section was composed of 500 measurements spaced at 5-mm (3/16-in.) intervals. Twenty profilometer transverse cross section measurements at 0.3-m (1-ft.) intervals were taken at each test window. Surface profile measurements were made at each traffic stop to define the progression of surface rutting throughout the traffic tests. Rut depth was defined as the difference between the surface depth at a given number of passes and the corresponding depth measured at zero passes. A typical surface rut measurement and the definition of maximum rut depth are shown in Figure 15. Traffic testing was terminated when the average maximum surface rut depth of 12.5 mm was reached or exceeded.
3. In addition to the profilometer measurements, elevation measurements were conducted with a rod and level prior to the start and at the end of the traffic tests for each test window. Elevations were monitored at locations were the profilometer legs were placed during profilometer measurements to detect any potential change in elevation that would affect the profile measurements. In addition, the elevation of the projection of vertical εmu stack on the asphalt surface was also monitored with a rod and level system. The results from the level surveys indicated that the profilometer leg points did not change elevation throughout the test.

Figure 13. Laser profilometer.

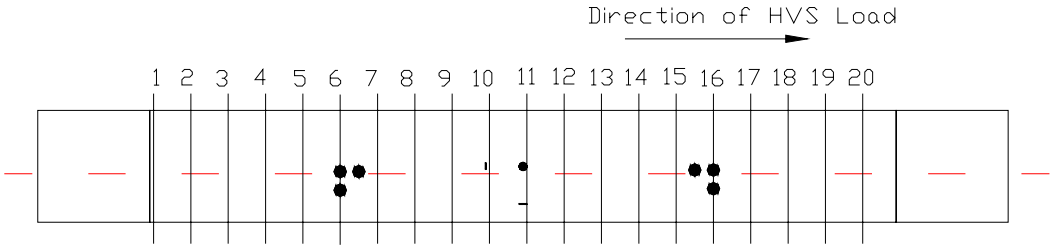

Figure 14. Locations for profile measurements in a test window.

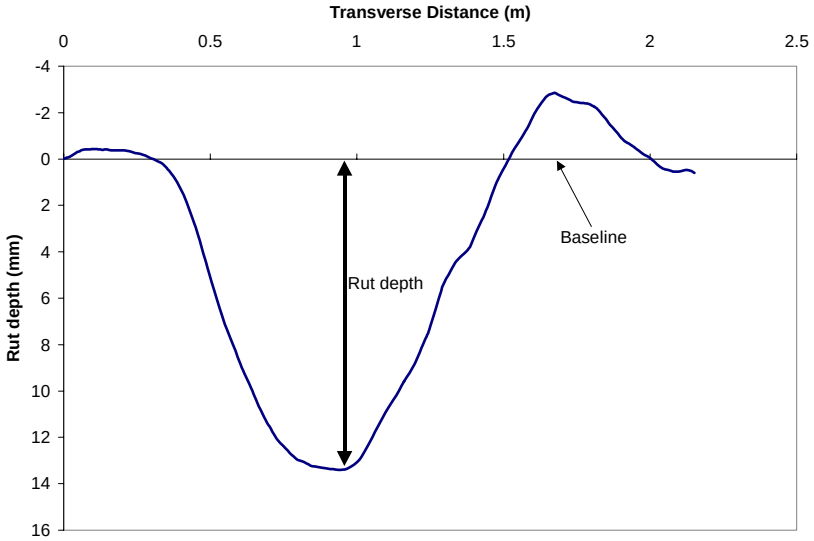

Figure 15. Definition of rut depth.

4. Subsurface stress and displacement measurements conducted in the vertical, longitudinal, and transversal directions relative to the direction of traffic. The measurements were conducted at various pass levels to define their progression throughout the traffic tests. The displacement measurements were conducted dynamically upon the passing of tire traffic, and also statically when no traffic was occurring. The dynamic displacements measured the resilient deformation during traffic load events. The static measurements provided a way to measure permanent deformation.
5. In addition to the εmu coils embedded in the pavement, a mobile coil was placed on top of the asphalt over a vertical stack of embedded εmu coils as shown in Figure 16. This provided a means to measure the vertical permanent deformation in the asphalt layer.

Figure 16. Measuring displacement between the AC surface and the top of the base course.

TRAFFIC LOADING

Traffic loading was applied by means of CRREL's Heavy Vehicle Simulator (HVS). The tire assembly was a dual-tire standard truck half axle. The traffic speed was 12 km/hr. The traffic was allowed to wander across a width of 0.91 m (3 ft.). The applied loads are summarized in Table 3. The tire pressure was set to 690-kPa (100 psi).

Table 3. Mean semi-axial loads on test windows

	Applied Loads	
Test Window	kips	kN
711C1	6	26.7
711C2	22	97.9
711C3	18	80
711C4	18	80
711C5	9/18	40/80
711C6	22	97.9

Table 4. Sequence of HVS tests on test windows

Window	Start	End
711C1	07-Feb-2005	18-Apr-2005
711C2	03-Aug-2006	05-Sep-2006
711C3	16-Nov-2005	07-Dec-2005
711C4	19-Sep-2006	15-Oct-2006
711C5	06-Jun-2005	09-Nov-2005
711C6	07-Sep-2006	18-Sep-2006

TEMPERATURE AND MOISTURE DURING TRAFFIC

The test section was built inside a facility where temperature and moisture were controlled. The mean air temperature during the traffic test period was 20ºC (68ºF). Thermocouples embedded in the asphalt concrete, the base course and the top of the subgrade indicated that the mean temperatures in the various layers of the pavement structure were practically the same as the air temperature. The temperature differences between this test section and other test sections in this study are very small, and therefore, variations in material properties due to temperature variations were insignificant. Temperature and moisture measurements were recorded at four-hour intervals. The moisture sensors were Campbell Scientific model CS615. These sensors measure the

oscillation frequency between two rods embedded in the moist soil. The oscillation frequency is related to the dielectric constant that changes with moisture content, and to a lesser degree with temperature. The sensor readings are also affected by salinity, mineralogy and presence of organic materials. Volumetric moisture content is converted to gravimetric moisture content through weight-volume relationships and soil specific gravity. Figure 18 shows the oven-dry corrected gravimetric moisture measurements in the base course, at 15 cm (6 in.) below the top of the subgrade and at 61 cm (2 ft.) below the top of the subgrade The moisture sensor data suggest that a small decrease in moisture content at the top of the subgrade, and a small increase in moisture at the lower subgrade location. The test section is built above a concrete floor, and it is surrounded by concrete wall and covered by 76 mm (3 in.) of asphalt concrete. Neglecting vapor diffusion through these very low permeability materials, one can consider the subgrade and base course system as a practically sealed system. Therefore, the small decrease in moisture content near the top of the subgrade must come as a result of moisture migration within the test section.

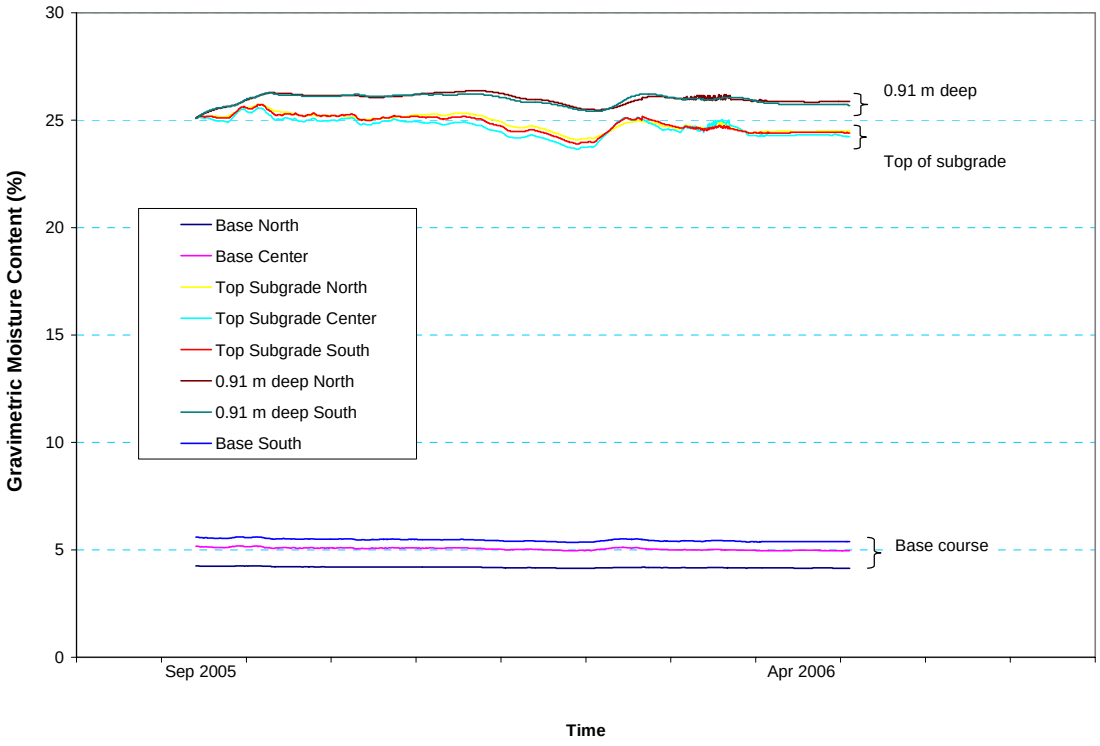

Figure 18. Moisture measurements in the base and subgrade during testing.

Figure 3 shows that, for this subgrade soil at 25 percent moisture content, the laboratory CBR value is approximately 13 percent. Figure 19 shows that this is equivalent to a resilient modulus (Mr) of 96.5 MPa (14 ksi). If the moisture content increases to 26 percent as originally intended for this test section, the laboratory CBR would be reduced to 9 percent, corresponding to an Mr value of 75.8 MPa (11 ksi).

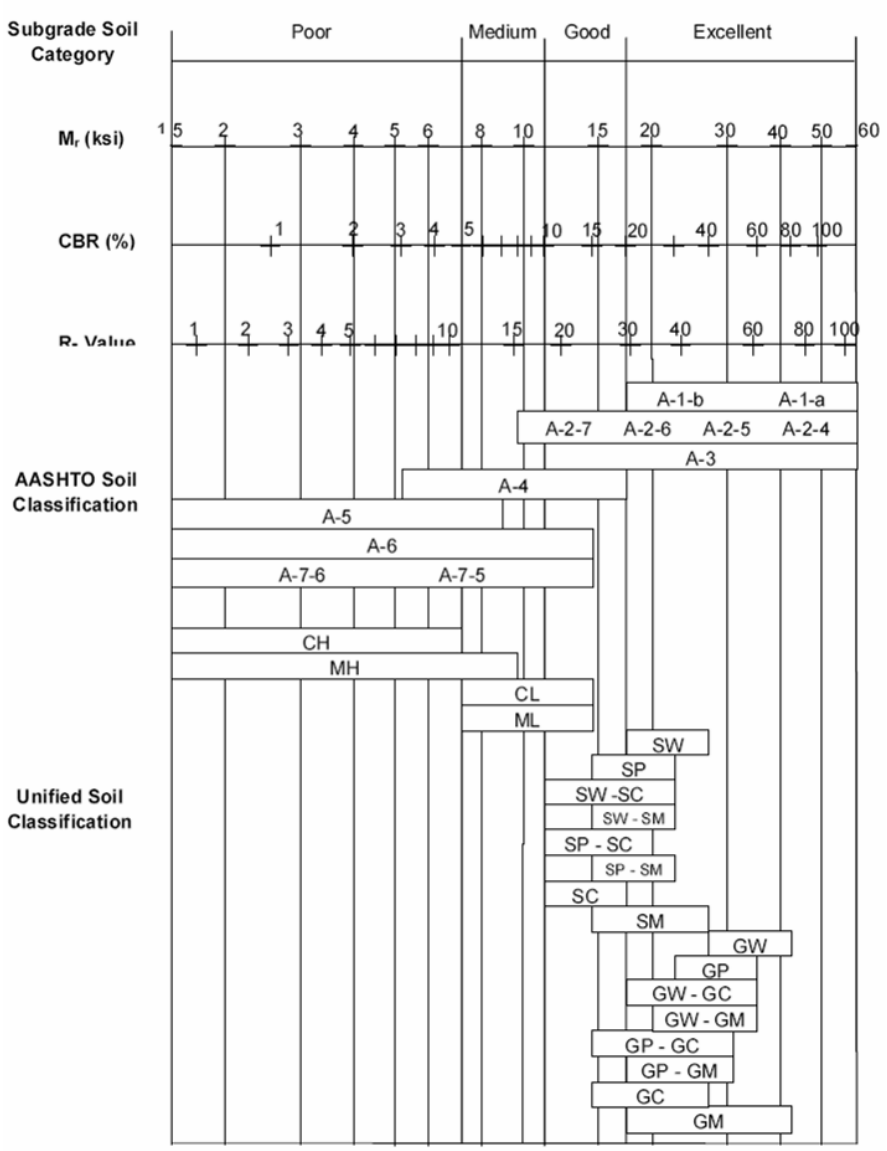

Figure 19. Relationships between CBR and resilient modulus for various soil types. (Proposed AASHTO M-E Guide, 2004).

SURFACE RUTTING

Transverse surface profile measurements were taken before HVS testing, at several intermediate numbers of traffic passes, and at the end of testing. Rut depth was calculated as the difference between the profile measurements taken at the given pass level and the profile measurements taken prior to testing (pass level zero). Cross sectional profile measurements were taken at 305-mm (1-ft.) intervals along the effective test window for a total of 20 locations. A laser profilometer scanning at 5-mm intervals was used to make the measurements. For each test window, the maximum rut depth at each cross section was used to assemble a longitudinal profile. Using the average rut depth of the 20 cross sections for each test window, Figure 20 shows the progression of rut depths

as a function of traffic repetitions for test windows subjected to various load intensities. The axial load intensity applied to each test window is also indicated in this figure. As expected, test windows tested with heavier loads deformed faster than those tested with lighter loads. The gravimetric moisture content of the subgrade soil in Test Section 711 was 25 percent. The modified Proctor optimum moisture content was 20.5 percent. Despite the higher moisture content Test Section 711 was relatively strong. Producing the desired rut depth of 12.7 mm (0.5 inch) became time and cost prohibitive. For example, Test Window 711c5 was tested with the standard axial load of 80 kN (18 kips). After 500,000 traffic repetitions, the rut depth was 5.2 mm. Therefore, for each test window, the number of traffic repetitions needed to produce 12.7 mm of rut depth had to be estimated by projecting the experimental curve. For Test Window 711c5 with the standard axial load, failure was estimated to occur at approximately 25 million traffic repetitions.

Figures 27 to 32 present longitudinal rut depth profiles for each test window as a function of load repetitions.

The semi-axial load applied to Test Window 711c1 was 26.7 kN (6 kips). This corresponds to an axial load of 53.4 kN (12 kips). Figure 20 shows that after 500,000 traffic repetitions this test window had developed a rut depth of only 2.5 mm. By projecting the experimental data curve it appears that this test section would require approximately 1 billion traffic repetitions to produce a rut depth of 12.7 mm (0.5 in).

The axial load applied to Test Window 711c3 was 160 kN (36 kips). This is twice the load intensity of a standard axial load. Even with this overload, after 100,000 traffic repetitions, the rut depth was 6.3 mm. By projecting the experimental data curve in Figure 20, the estimated number of traffic repetitions needed to produce a rut depth of 12.7 mm was 2.2 million.

No cracking was observed in any of the test windows of Test Section 711. This was probably due to the relatively strong subgrade. The subgrade gravimetric soil moisture content was 25 percent compared to 20.5 percent optimum moisture content. A test section from a previous study (Perkins and Cortez, 2005) was built with this subgrade soil at 29 percent gravimetric moisture content. During construction, the soil became unworkably sticky and unstable at some locations were minor increments of moisture content existed. Although this subgrade soil is relatively strong for a wide range of moisture contents, past a critical value, it becomes weak even with small increments of moisture content. Figure 2 shows that this soil contains 33 percent of soil particles within the clay particle size range. This clay content is sufficient for the clay particles to govern the mechanical behavior of the soil mass.

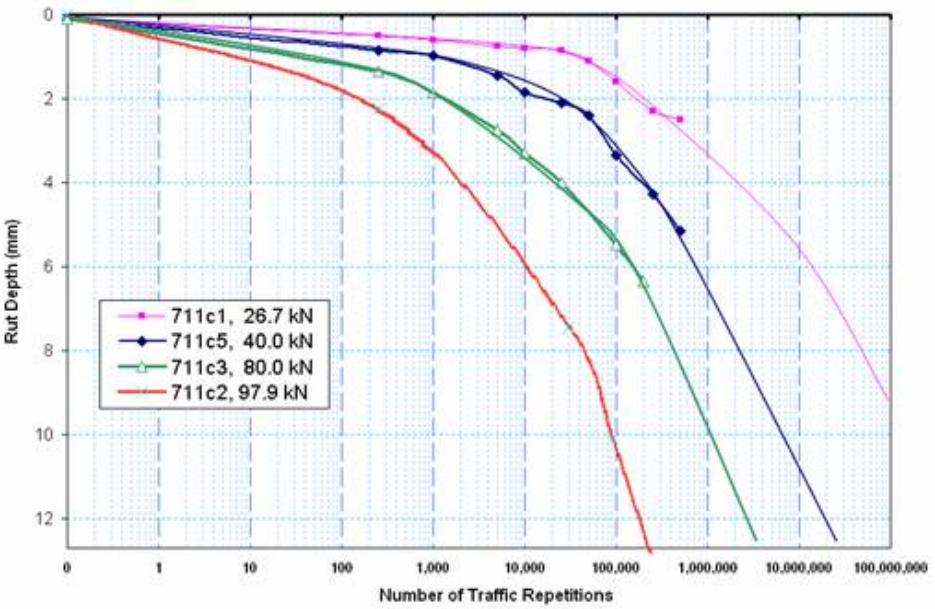

Figure 20. Average rut depth as function of traffic load repetitions and semi-axial load intensity.

Figure 21. Test Window 711c1 before HVS traffic.

Figure 22. Test Window 711c1 at the end of HVS traffic.

Figure 23. Test Window 711c2 before HVS traffic.

Figure 24. Test Window 711c2 at the end of HVS traffic.

Figure 25. Test Window 711c3 before HVS traffic.

Figure 26. Test Window 711c3 at the end of HVS traffic.

Figure 27. Test Window 711c5 before HVS traffic.

Figure 28. Test Window 711c5 at the end of HVS traffic.

During traffic testing of Test Window 711c5, a slowly dripping oil leak developed. The leak was repaired but the surface of the effective test window had a sticky appearance. However, there was no evidence of asphalt softening beyond a very thin surface layer.

At the end of 500,000 passes with a standard axial load of 80 kN (18 kips), the load was doubled and 250,000 additional traffic passes were applied. Figure 27 is a modified copy of Figure 20 that includes the additional traffic passes with the increased load.

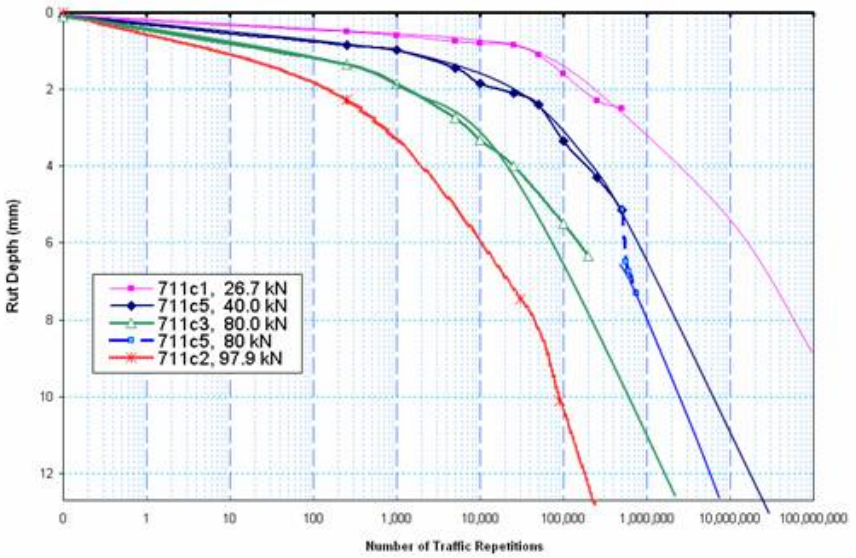

Figure 29. Average rut depth as function of traffic load repetitions and semi-axial load intensity, including additional, heavier traffic on Test Window 711c5.

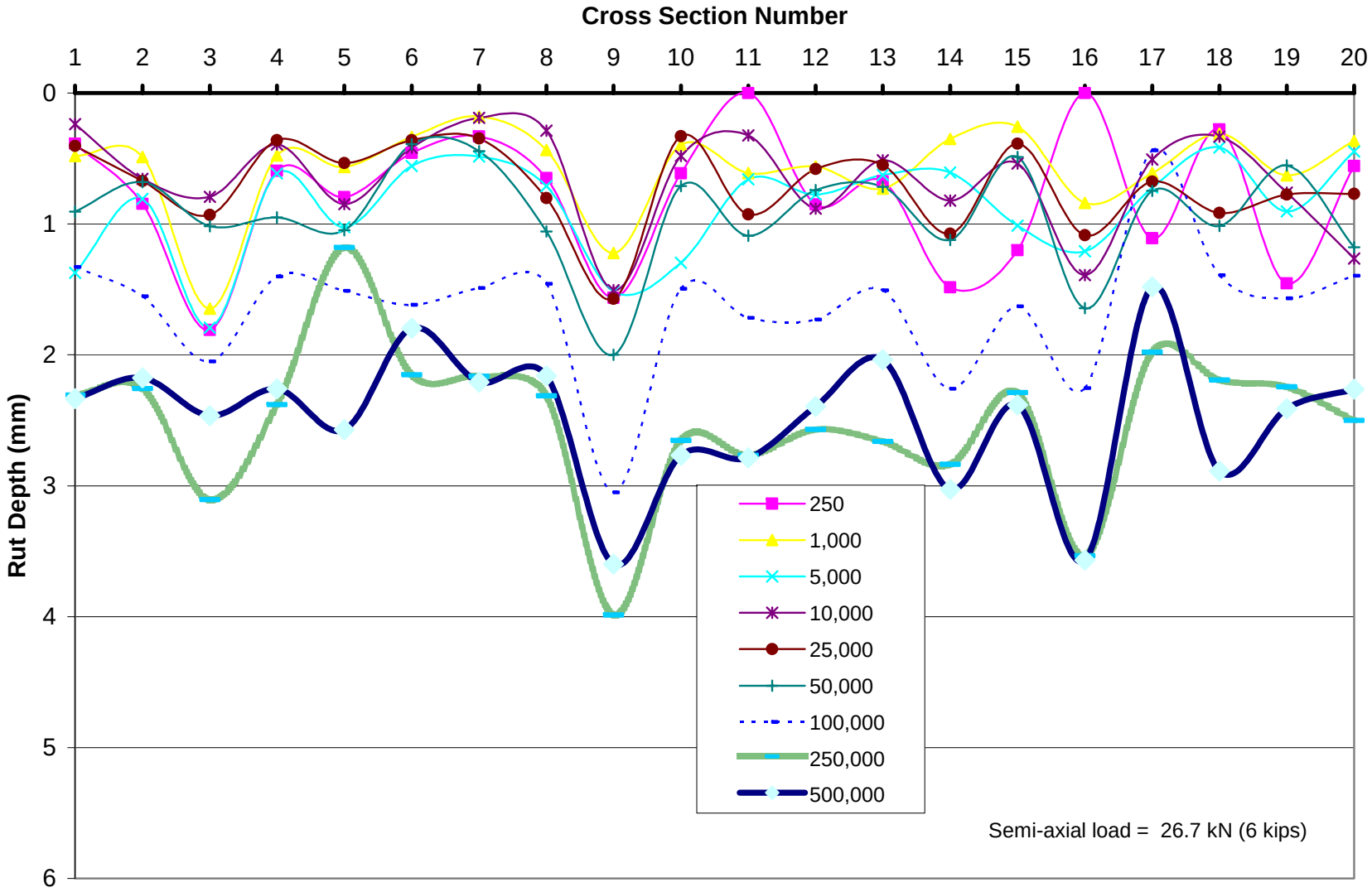

Figure 30. Progression of surface rutting along the center of the tire path in Test Window 711c1.

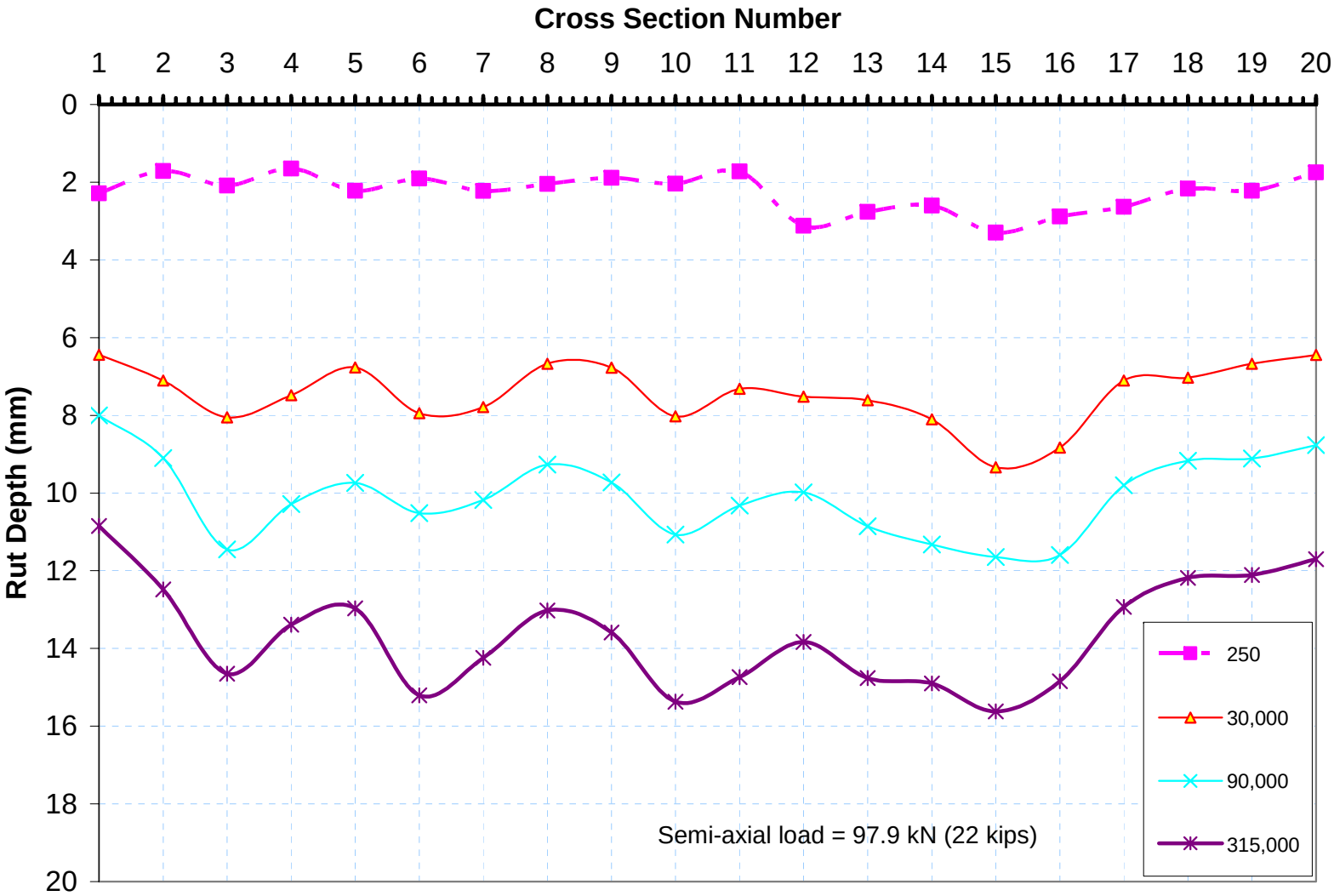

Figure 31. Progression of surface rutting along the center of the tire path in Test Window C2.

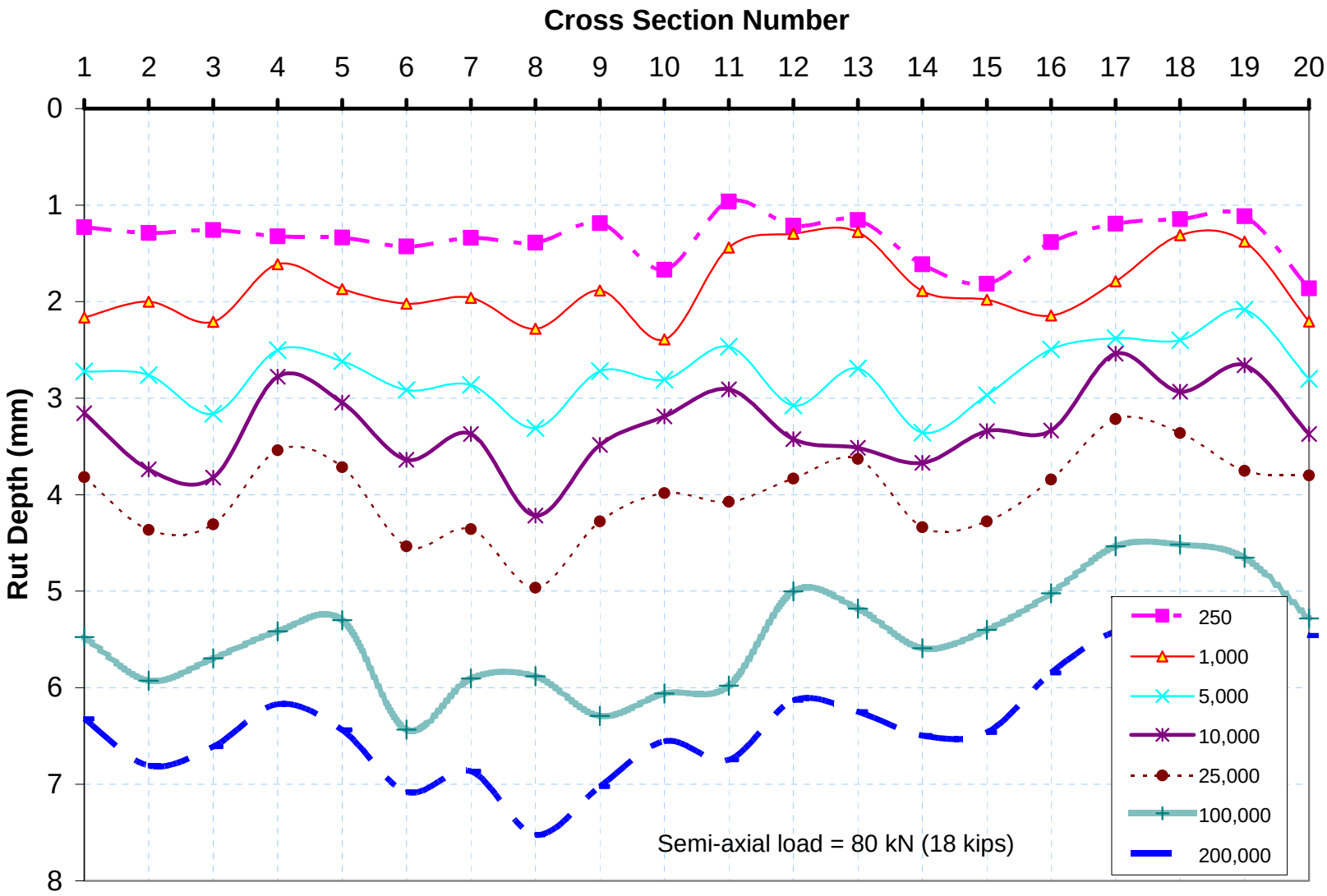

Figure 32. Progression of surface rutting along the center of the tire path in Test Window 711c3.

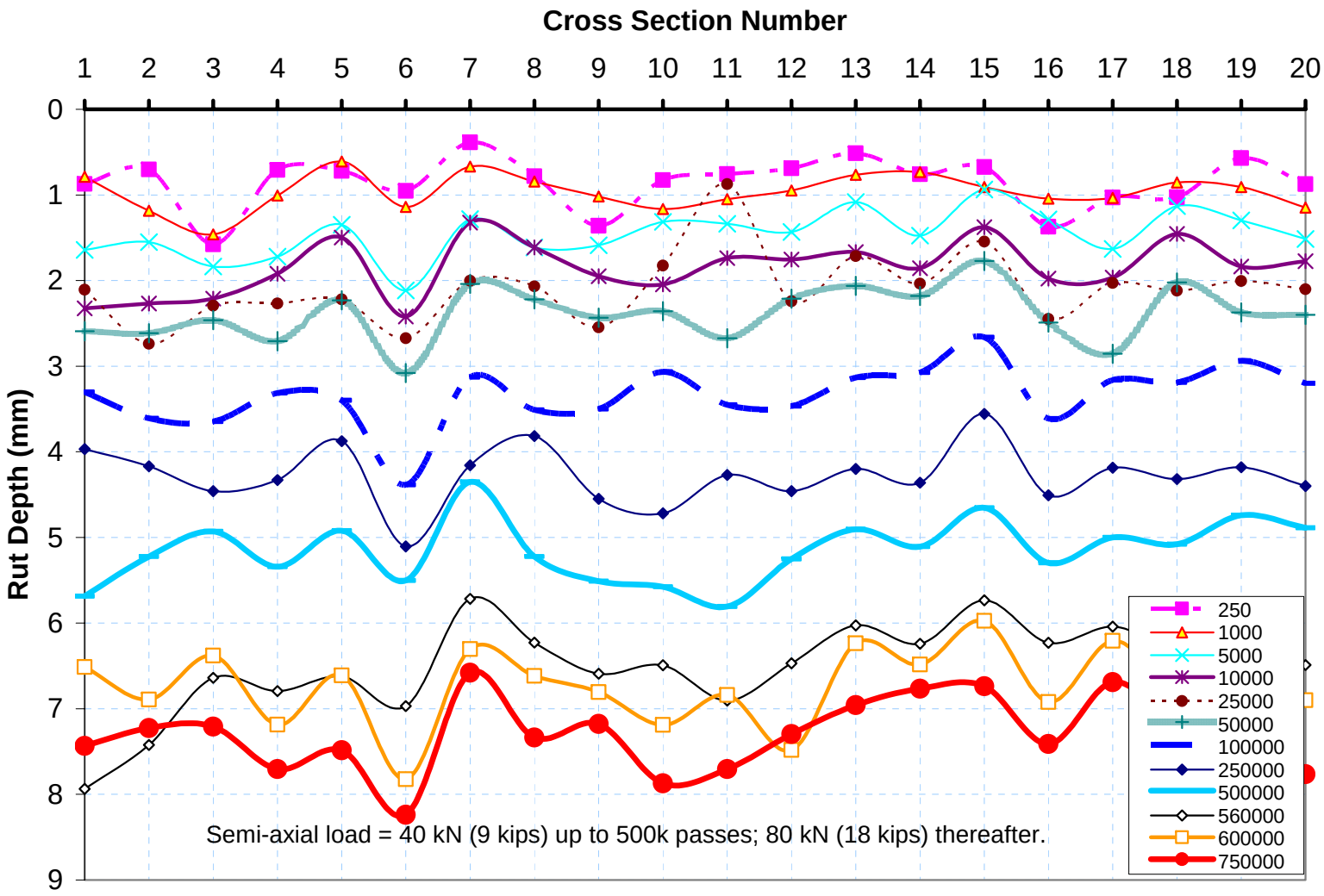

Figure 33. Progression of surface rutting along the center of the tire path in Test Window 711c5.

Table 8 shows the number of traffic passes required to cause a rut depth of 12.7 mm (0.5 in) estimated from the projections of the experimental data. Figure 34 graphically shows the relationship between load intensity and number of traffic passes to failure, and also a power function that fits the experimental data with an R^2 value of 0.93.

Table 8. Load Repetitions to reach failure of 12.7 mm

Test Window	Load (kN)	$N_{failure}$
c1	26.7	1,000,000,000
c5	40.0	30,000,000
c3	80.0	4,00,000
c2	97.9	220,000

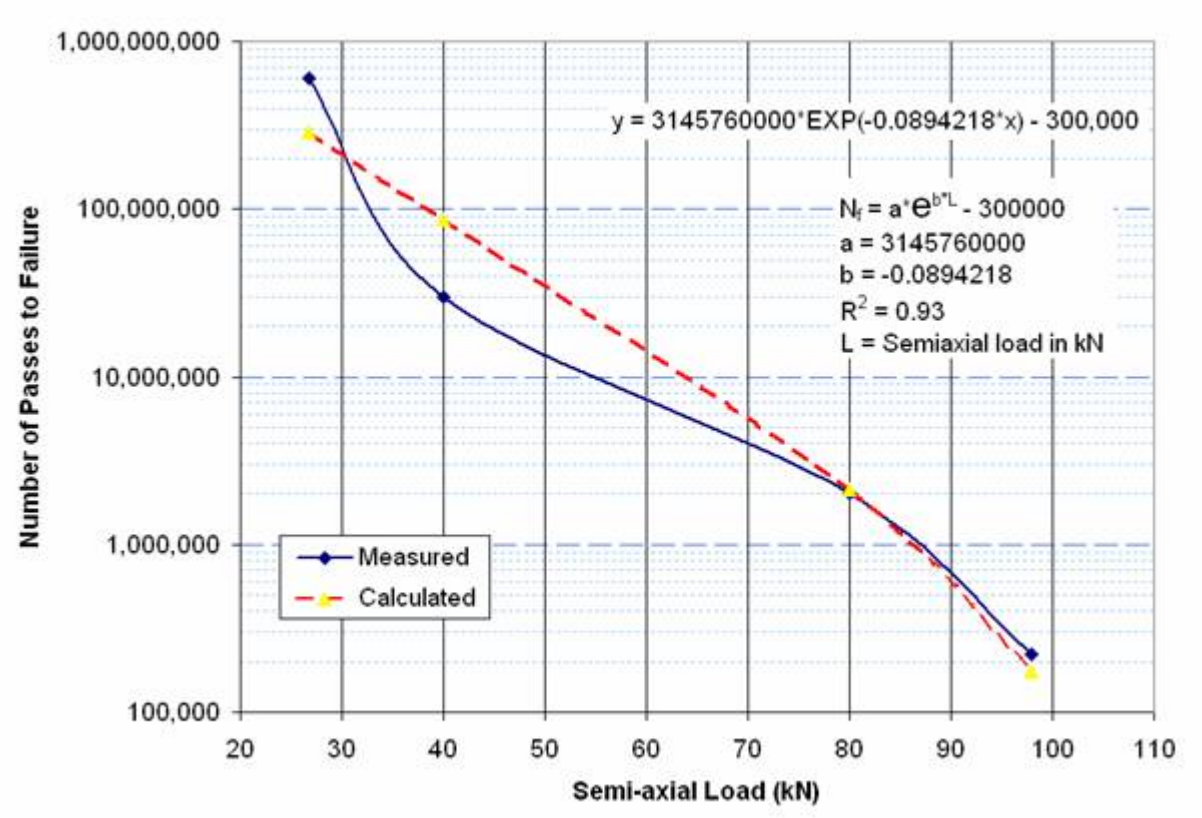

Figure 34 Load repetitions to failure as a function of load intensity.

DEFORMATION AND STRAIN

Ɛmu inductance coil sensors were used to measure the distance between pairs of coils at various stages throughout the traffic testing. Comparing the distance between a pair of coils to the initial distance, the deformation of the soil between the coils can be established. An average strain value can then be calculated by dividing this deformation by the initial coil distance. By convention, we assign this strain value to a point located in the middle between the coil pair. Coil distance measurements were conducted at stages

with the HVS stopped to obtain permanent deformation, and also dynamically during traffic applications to obtain resilient deformations.

a) Permanent Deformations

Permanent deformation measurements were collected from εmu coils embedded in the base and the subgrade. Measurements were conducted before traffic began and at various stages throughout the traffic tests. An additional mobile εmu coil was placed at the asphalt surface and paired with a coil embedded just below the bottom of the asphalt concrete (AC) to measure the vertical deformation that occurred in the asphalt layer. Three stacks of εmu coils were embedded to form triaxial arrangements in the base and subgrade. Vertical pairs of εmu coils were embedded down to a depth of 1.52 m (5 ft) from the asphalt surface. Previous experiments have shown that, at this depth, the strains are normally small compared to electronic noise.

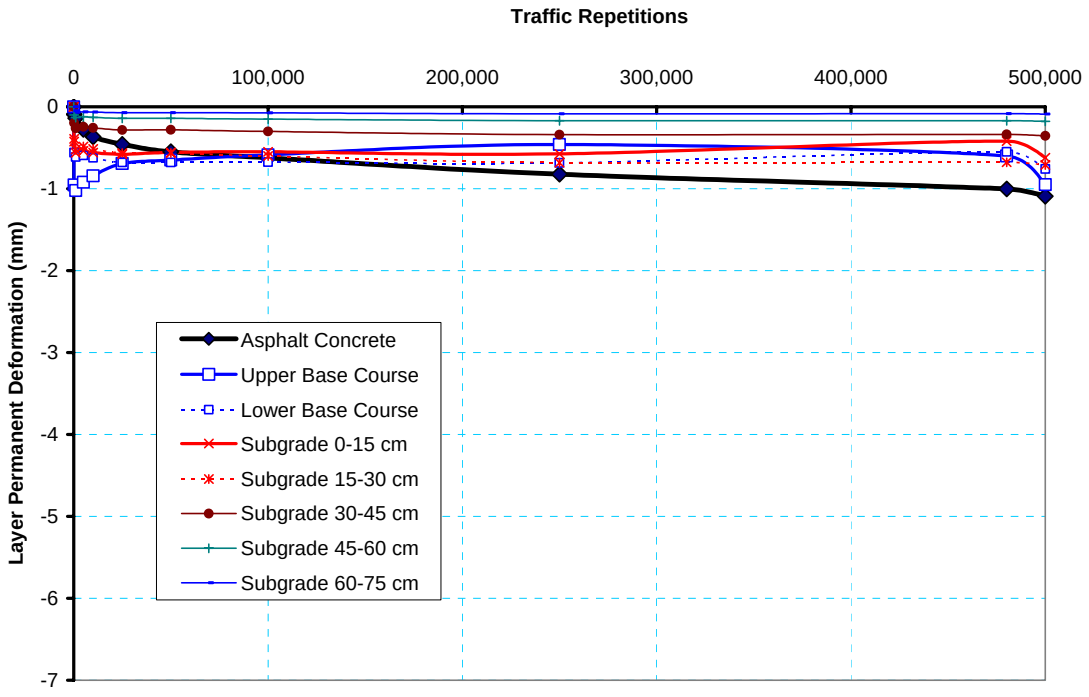

Figure 35a. Layer by layer vertical permanent deformation in Test Window 711c1 with 26.7 kN semi-axial load.

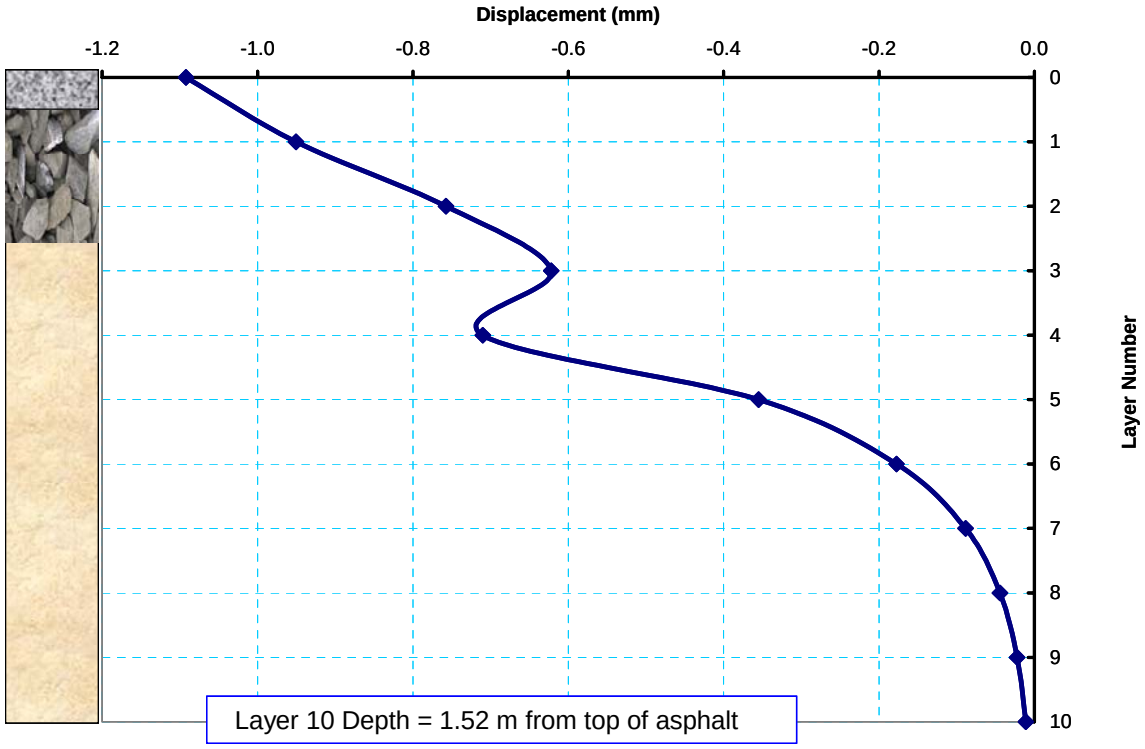

Figure 35b. Layer by layer vertical permanent deformation at failure in Test Window 711c1 with 26.7 kN semi-axial load.

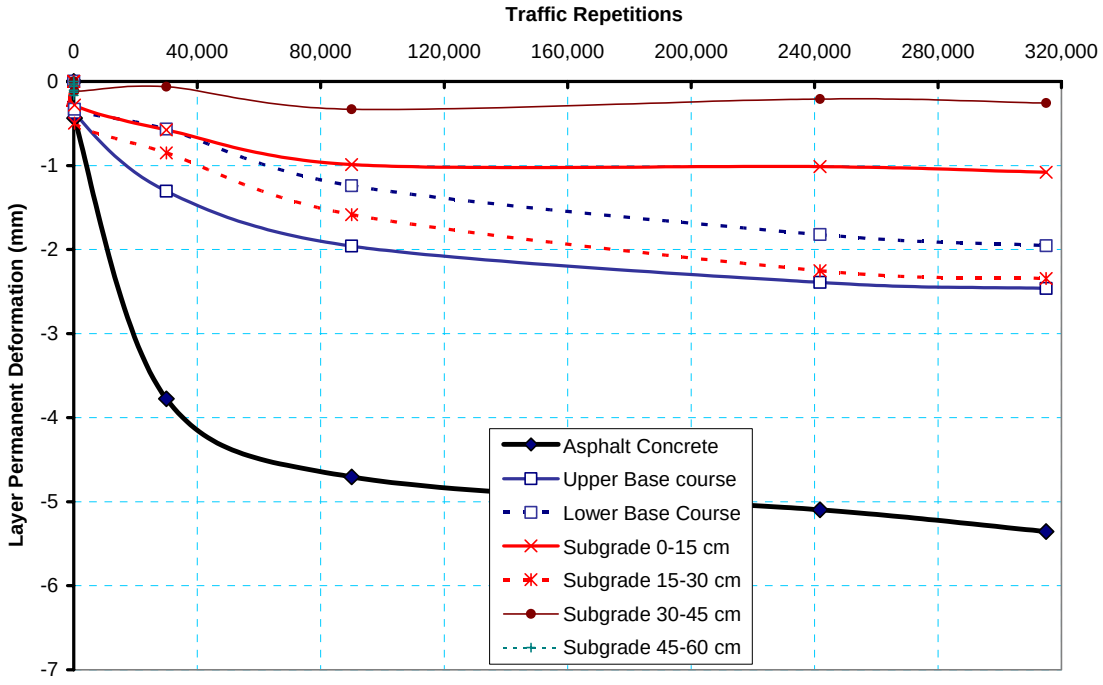

Figure 36a. Layer by layer vertical permanent deformation in Test Window 711c2 with 97.9 kN semi-axial load.

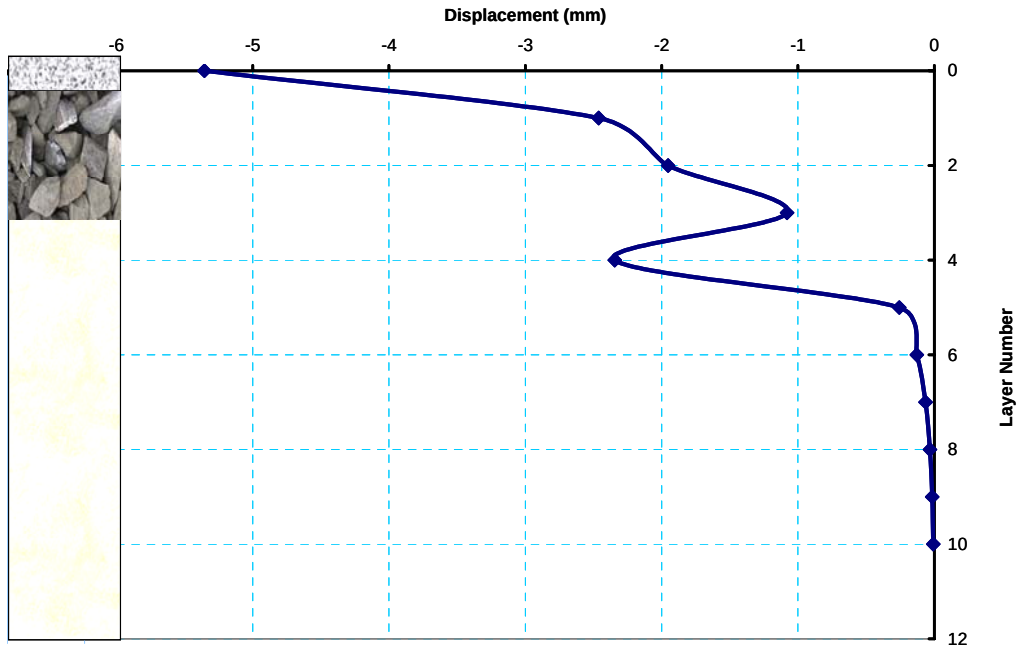

Figure 36b. Layer by layer vertical permanent deformation at failure in Test Window 711c2 with 97.9 kN semi-axial load.

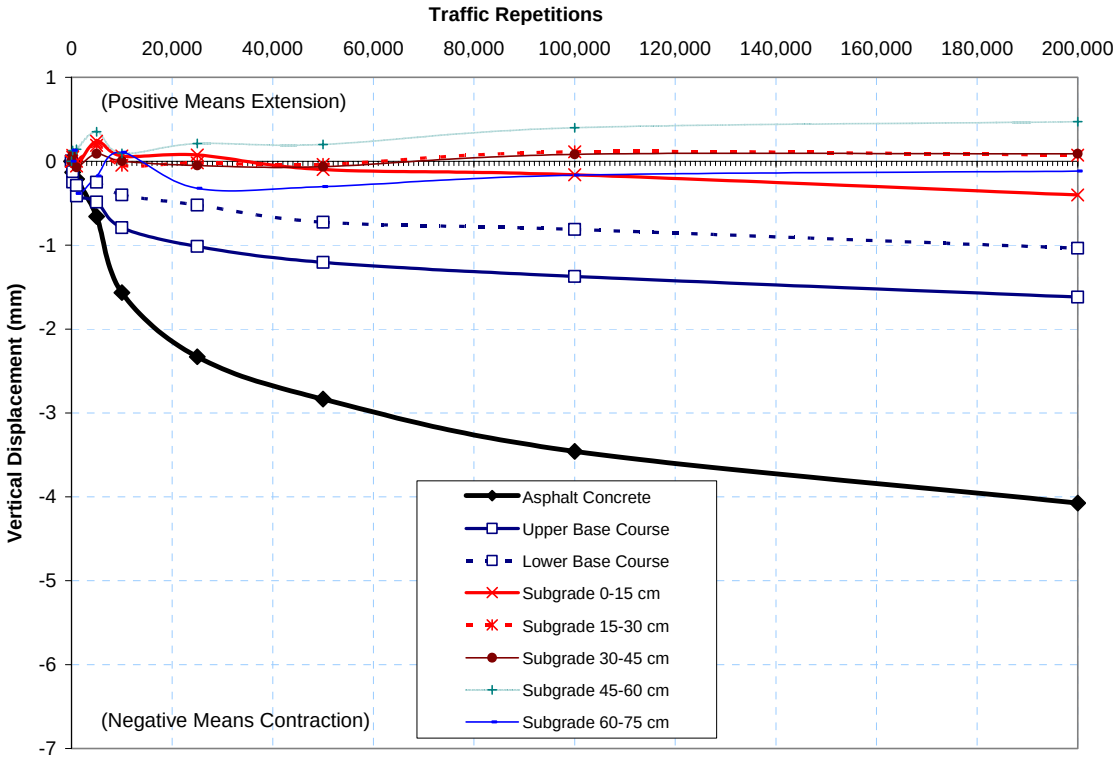

Figure 37a. Layer by layer vertical permanent deformation in Test Window 711c3 with 80 kN semi-axial load.

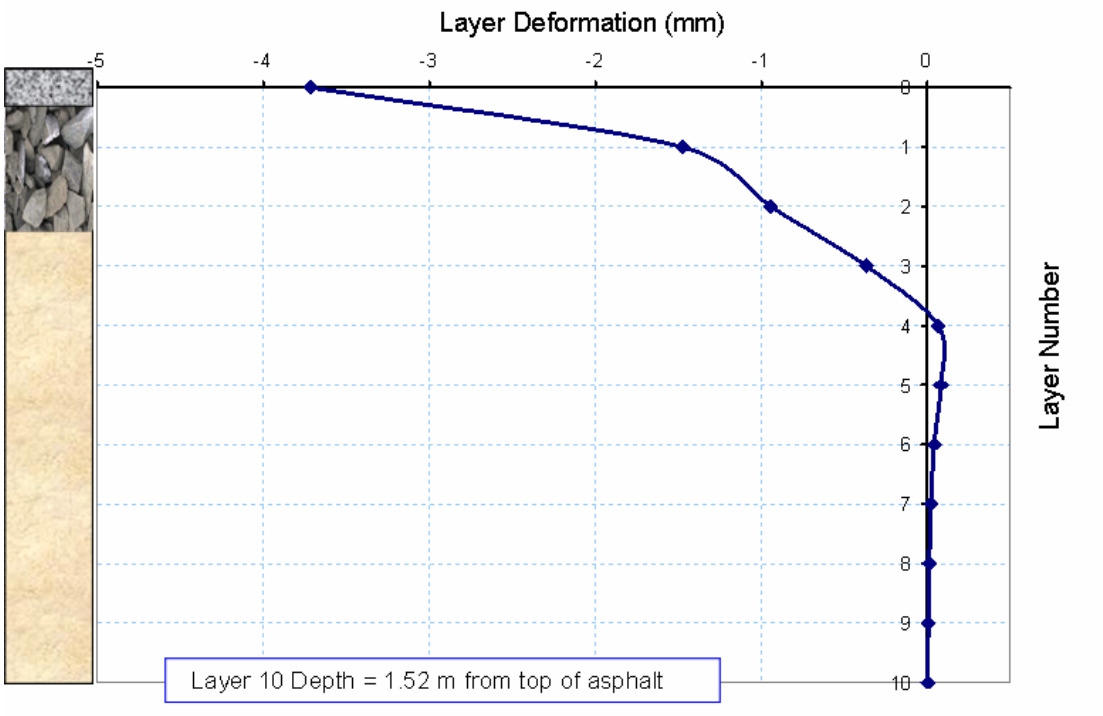

Figure 37b. Layer by layer vertical permanent deformation at failure in Test Window 711c3 with 53.4 kN semi-axial load.

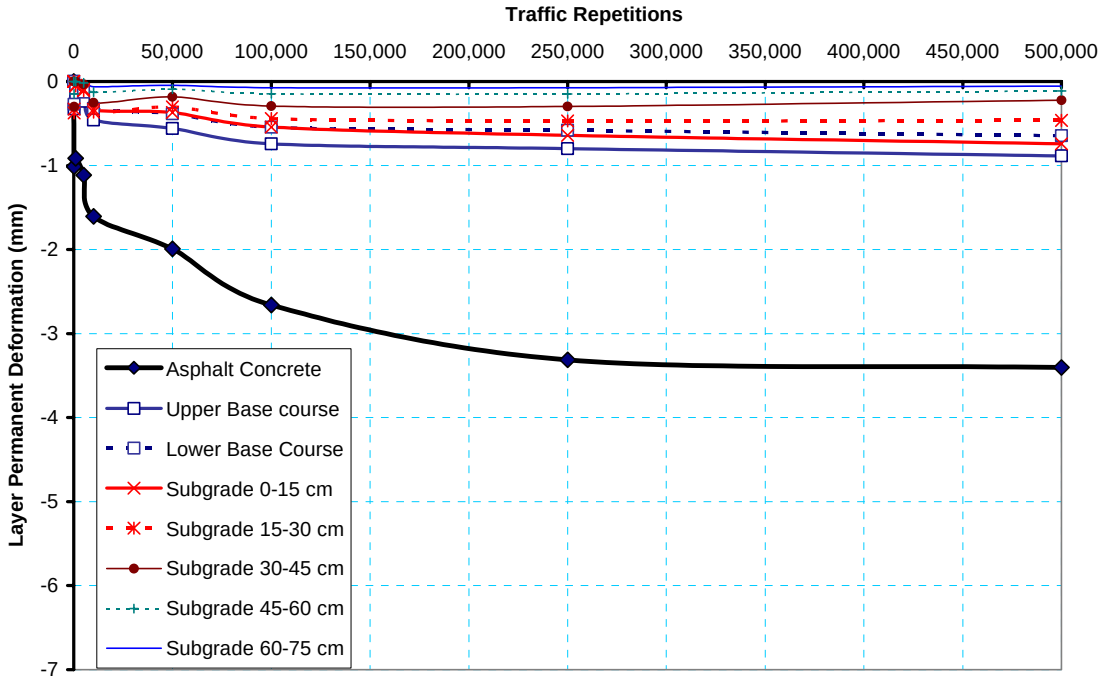

Figure 38a. Layer by layer vertical permanent deformation in Test Window 711c5 with 40 kN semi-axial load.

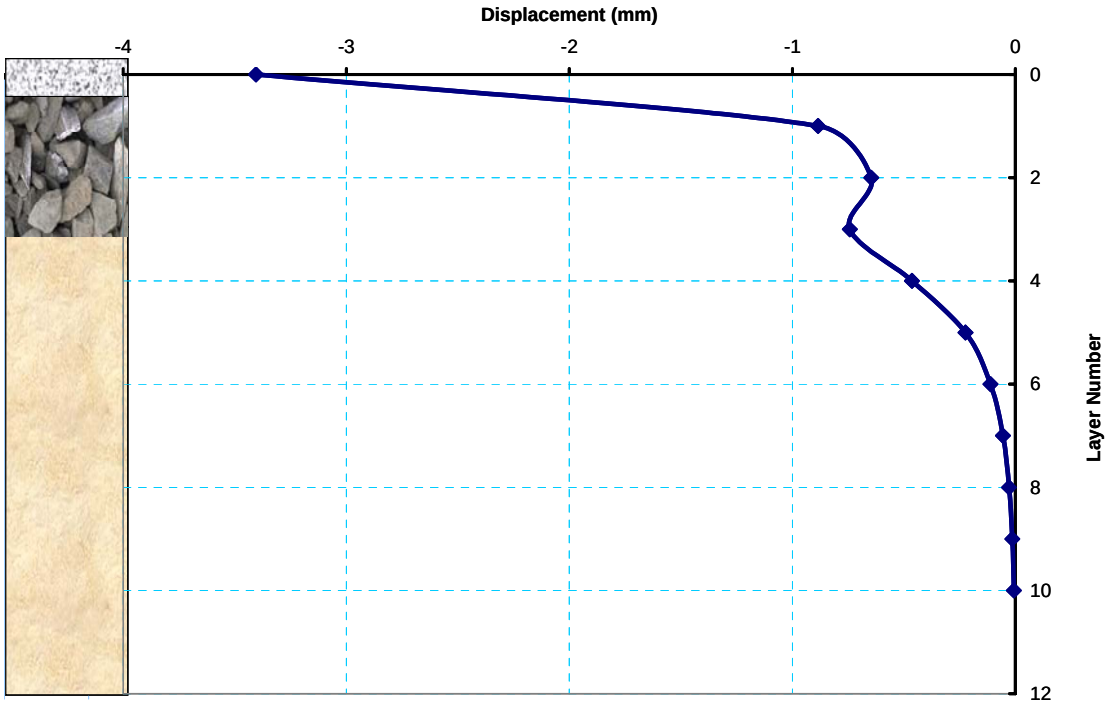

Figure 38b. Layer by layer vertical permanent deformation at 500,000 traffic repetitions in Test Window 711c5 with 40 kN semi-axial load.

The vertical permanent deformations in the top 15-cm layer of the subgrade as a function of load repetitions are shown in Figure 41. Negative deformation indicates contraction (i.e., decrease in distance between a pair of coils). The deformations within the top 15-cm layer were too small to be significant compared to the signal noise. Therefore, no reliable relationship can be established from the measurements in this layer alone. This graph is presented here only to allow comparison with corresponding graphs from other test sections.

b) Resilient Deformations and Strains

As with previous test sections, resilient deformations were measured with the εmu coil gages in two layers in the base course and eight layers in the subgrade. The vertical resilient deformations and strains were compressive. The transverse resilient deformations and strains were extensive. The longitudinal resilient deformations and strains were initially compressive until the tire assembly was located directly above the sensors, and thereafter suddenly reversed into extensive deformations and strains. Resilient deformations are induced by the dynamic rolling of the truck tires over the pavement test section and over the sensors. Observing the static permanent deformation and the dynamic measurements, one can conclude that for each traffic load event, most deformation is recoverable (resilient), but a small component of (permanent) deformation

remains and cumulates with traffic repetitions. However, the ratio of permanent to resilient deformations decreases when the number of traffic repetitions increases. This report will focus on vertical stress and strains. A later report will examine relationships between vertical and horizontal components of stress and strain in order to model soil behavior, and define the mechanical behavior of the pavement structure as affected by multiple parameters.

In general, resilient deformation and strain increased in proportion to the traffic load intensity. Resilient strains as a function of load repetition at 76 mm (3 in.) below the top of the subgrade are presented in Figure 39. It can be seen that the resilient strains increased with the number of traffic repetitions (strain hardening). This trend was more clearly observed in the test windows with higher load intensities.

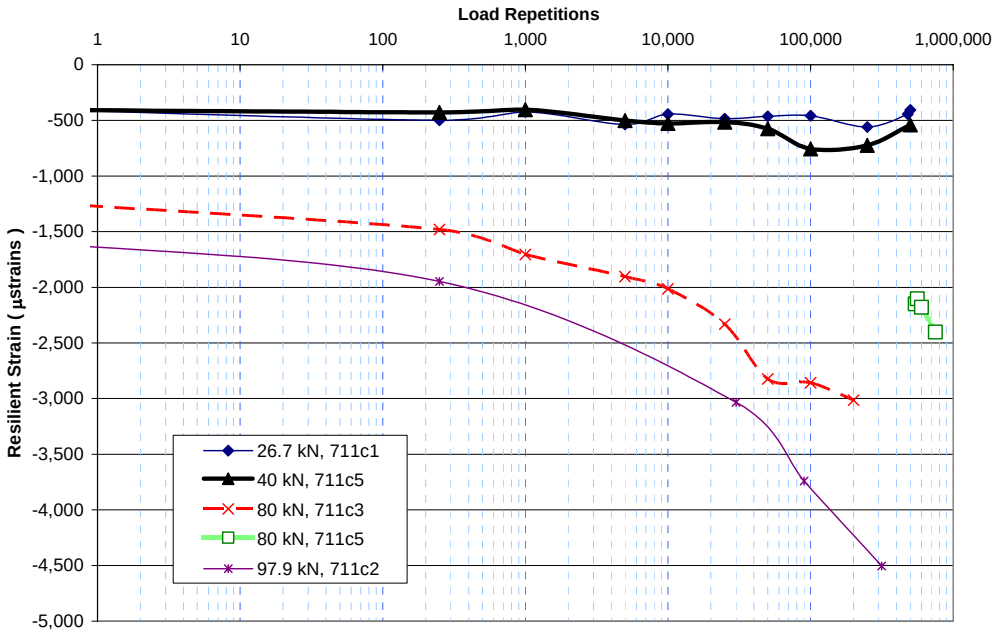

Figure 39. Resilient vertical strains 76 mm (3 in) below the top of subgrade for various semi-axial traffic loads.

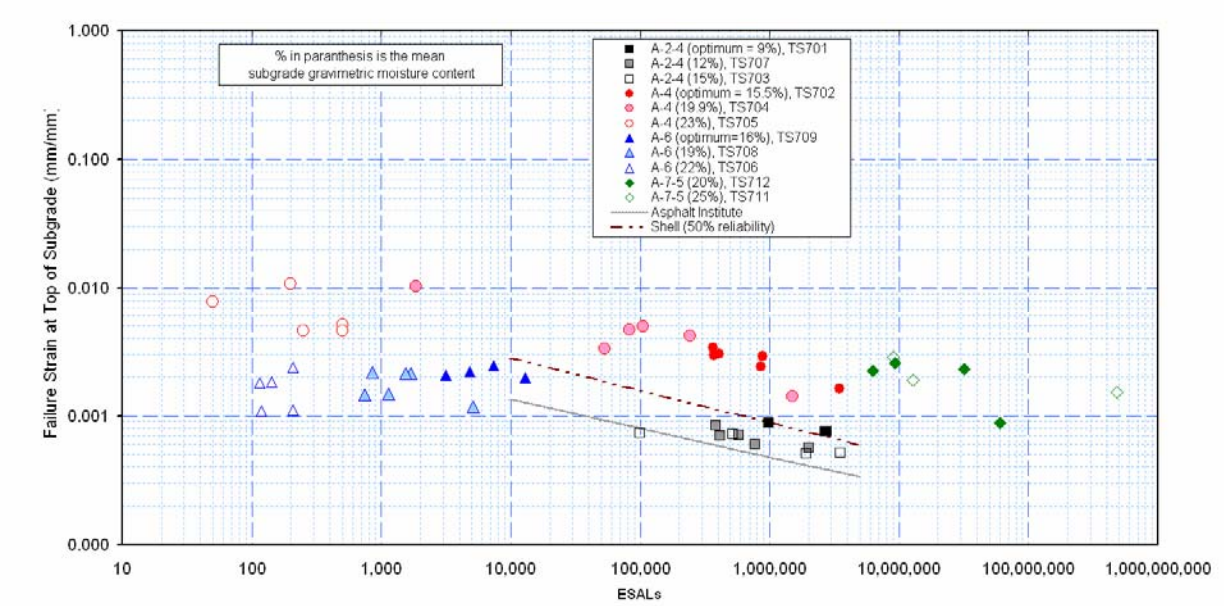

Figure 40. Effect of soil type and moisture content on subgrade failure criteria.

Figure 40 shows the resilient strain at the top of the subgrade at failure for all the subgrade soils included in this study. The existing subgrade failure criteria established by the Asphalt Institute and the Shell corporation are also graphed for comparison. It can be seen that the resilient behavior of the subgrade soil A-2-4 is consistent with the two established criteria, but significant differences occur for other soils. The data suggests that subgrade resilient strain criteria must be tailored to soil type.

STRESS

Stress measurements were conducted by means of Geokon® and Dynatest® gauges. All the stress gauges in the unbound granular base course were Geokon. The subgrade was instrumented with both stress gauge types. Figure 40 shows the stress measurements the middle of the base course in Test Window 711c5. The semi-axial load was 40 kN (9 kips).

In most cases, stress increased slightly with traffic repetitions. This is probably due to packing of soil particles under the action of traffic.

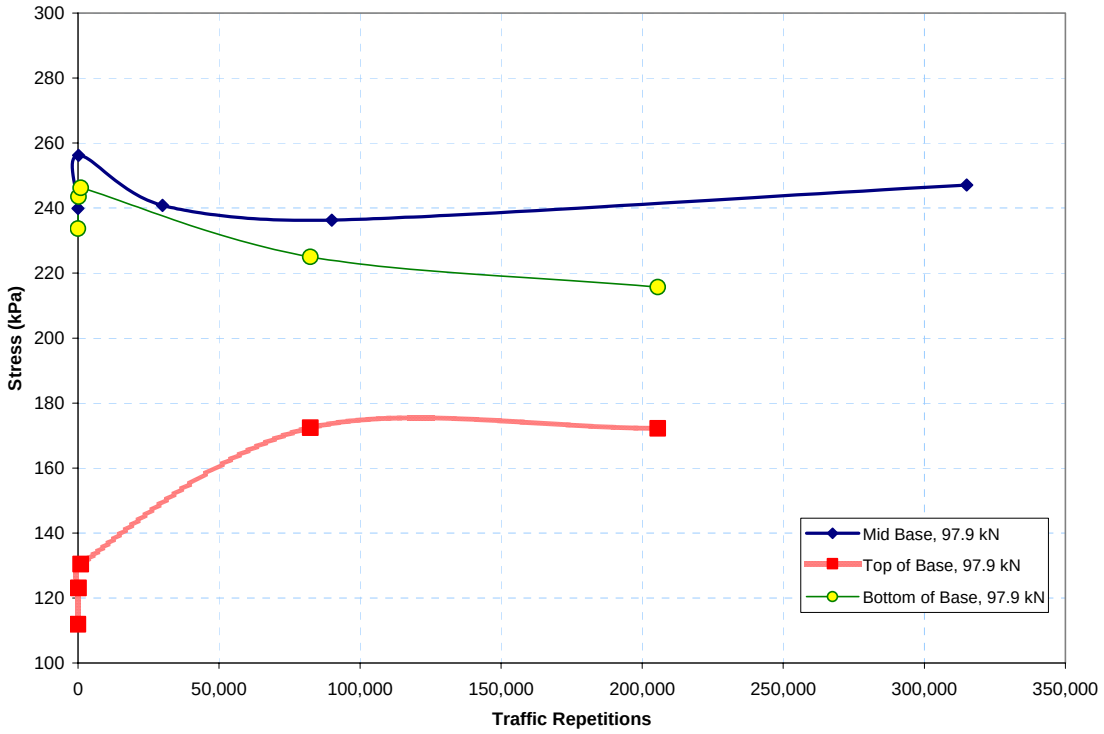

Figure 41. Stress measurements in the base course in Test Windows 711c2 and 7119c6, both with 97.9 kN semi-axial load.

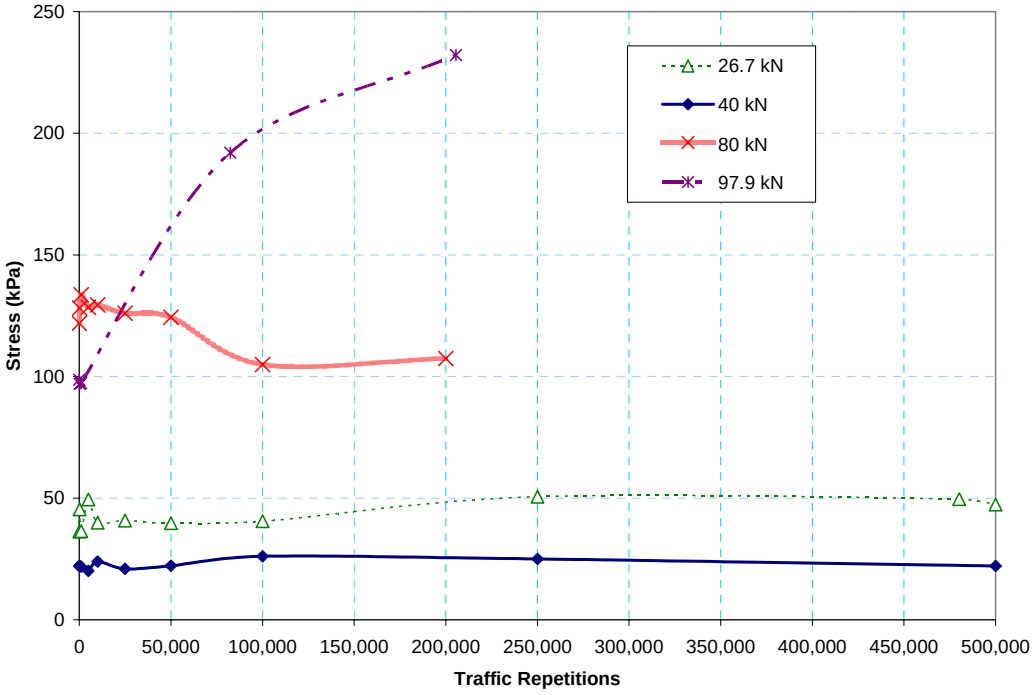

Figure 42. Vertical stress measurements at a depth of 76 mm below the top of the subgrade for four semi-axial load intensities.

FORENSIC EVALUATION

A forensic evaluation was conducted to establish the condition of the pavement structure at the end of the traffic tests. Two trenches were cut across the test windows. One trench was excavated across test windows 1, 2, and 3 on the south region of the test section. This trench will be referred to as the “South Trench”. Another trench was excavated in the north region of the test section. This trench cut across test windows 4, 5, and 6. The boundaries of the trenches were carefully located and marked to avoid damaging the embedded sensors and wires. Dry saw cutting was used to avoid disturbing the base and subgrade moisture contents. Base course and subgrade soil samples were taken immediately after exposure to determine their moisture contents by the oven-dry method. The side surfaces were carefully scrapped and dusted off to be able to measure asphalt and base layer thickness.

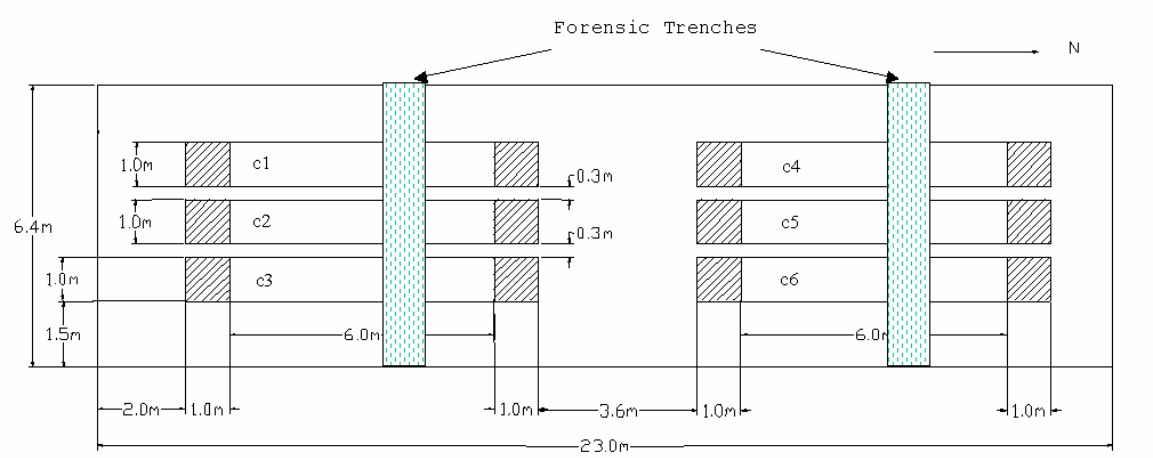

Figure 43. Location of the forensic trenches in Test Section 712

Figure 44 shows a view of the test section at the end of traffic. Except for Test Window 711c6, the only noticeable distress mode in all the test windows was smooth rutting. Test Window 711c6 experienced accelerated rutting at its south end. The asphalt on the sides of the traffic area bulged as shown in Figure 45.

Figure 44. View of test section at the end of traffic tests.

Figure 45. Soft spot and premature rutting in Test Window 711c6.

Moisture and density measurements were conducted inside the trenches in the base course and in the upper subgrade down to a depth of 0.91 m (3 ft.) below the top of the asphalt concrete. Figure 46 and 47 show the gravimetric moisture contents in the south and north trenches respectively. The measured values are consistent with those obtained during the construction, but the moisture content in the zone near the top of the subgrade experienced a drop of 2 to 3 percent in moisture content from the values measured during the construction. Figures 48 and 49 show density measurements for the south and north trenches at each test window and also at locations outside the traffic areas at the east and west sides of the test windows. Most measured values are above 90 percent of modified Proctor density.

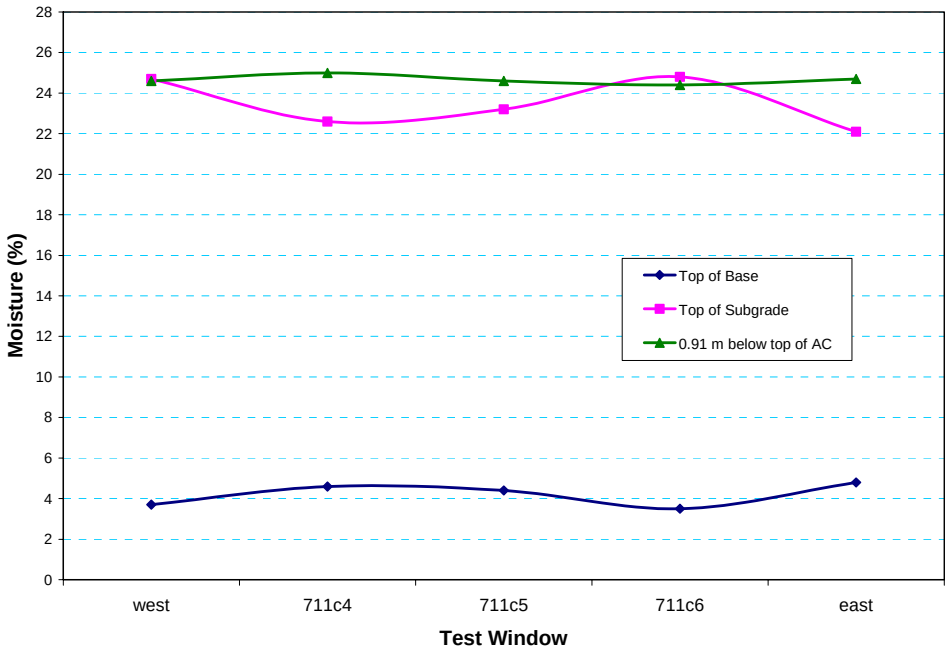

Figure 46. Moisture content in the base and upper subgrade in the south trench.

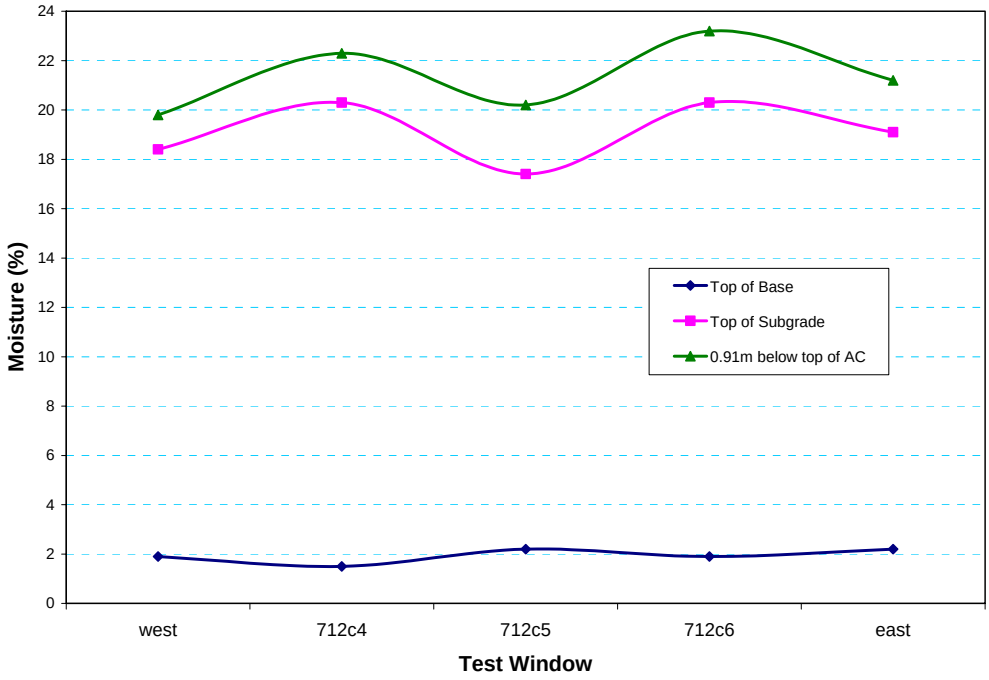

Figure 47. Moisture content in the base and upper subgrade in the north trench.

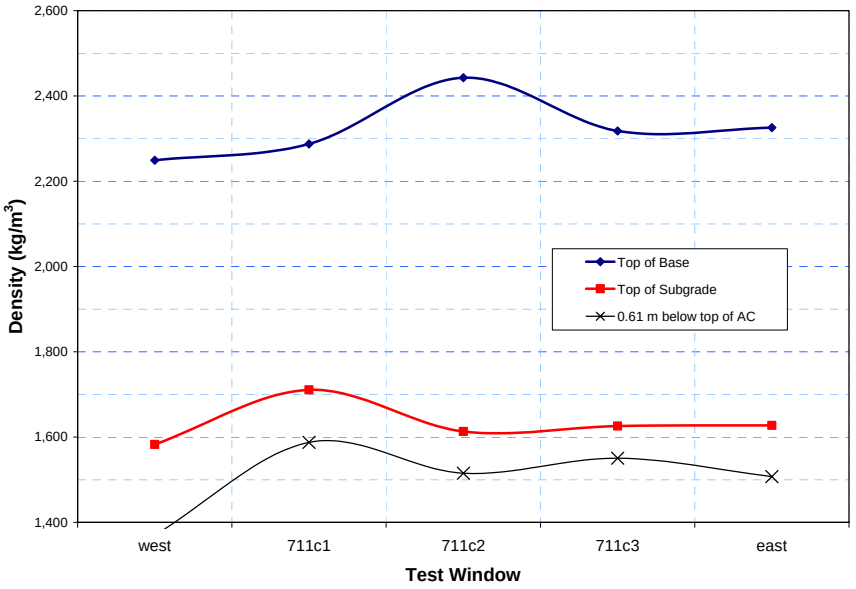

Figure 48. Density measurements in the base and subgrade in the south trench.

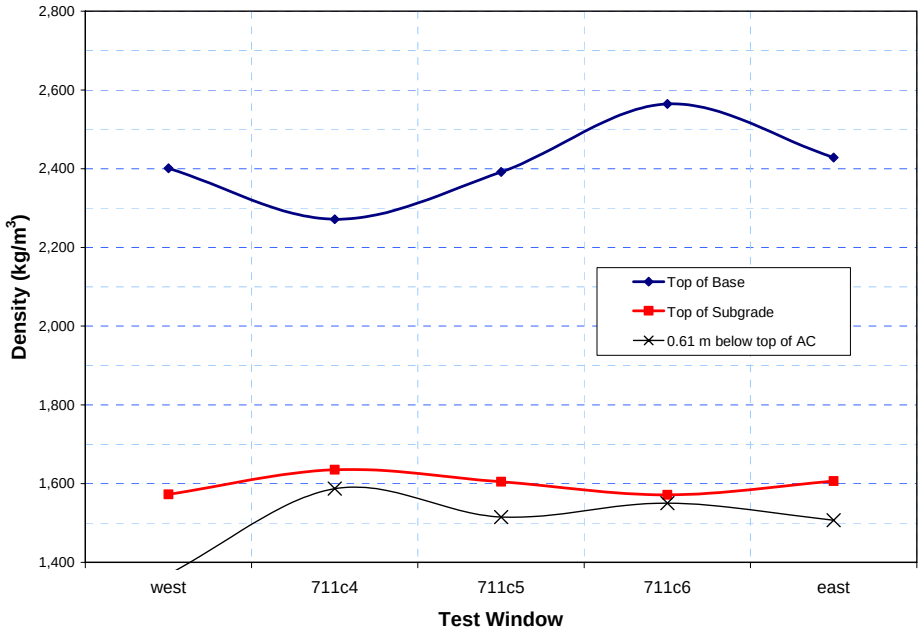

Figure 49. Density measurements in the base and subgrade in the north trench.

Asphalt and base course layer thickness measurements for each test window are presented in Figures 50 through 55. In Test Windows 712c1 and 711c2 the asphalt thickness was approximately as thick as intended. The average base course was also very close to its design value of 229 mm (9 in.).

In Test Window 712c3, the asphalt thickness was at the target value, but the base course was slightly thinner than intended.

In Test Window 712c4 the asphalt was significantly thicker than intended. This fact must be considered in the data analysis. The base thickness was slightly thicker than planned.

In Test Window 712c5 the average asphalt thickness was larger than planned, but the base course was on target

Test Window 712c6 had the largest deviations from design thickness for both the asphalt and the base layers. This fact must be considered in the data analysis. The irregular thickness may have contributes to a premature failure seen at the pavement surface as localized rutting and bulging of the sides of the traffic area. Rutting was relatively uneven in this test window.

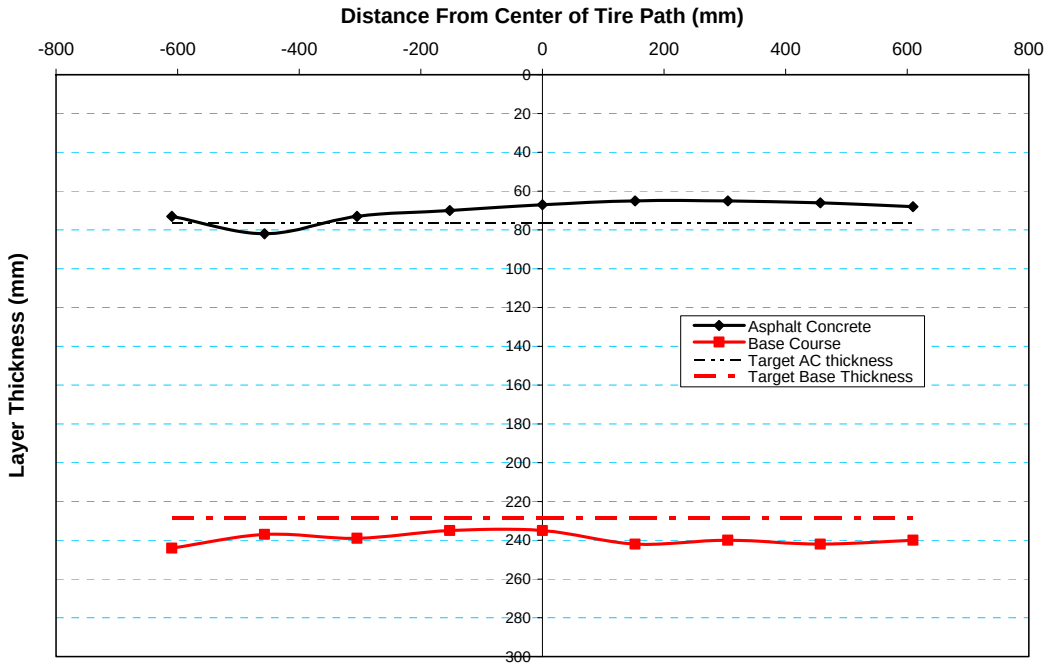

Figure 50. Layer thickness measurements across Test Window C1.

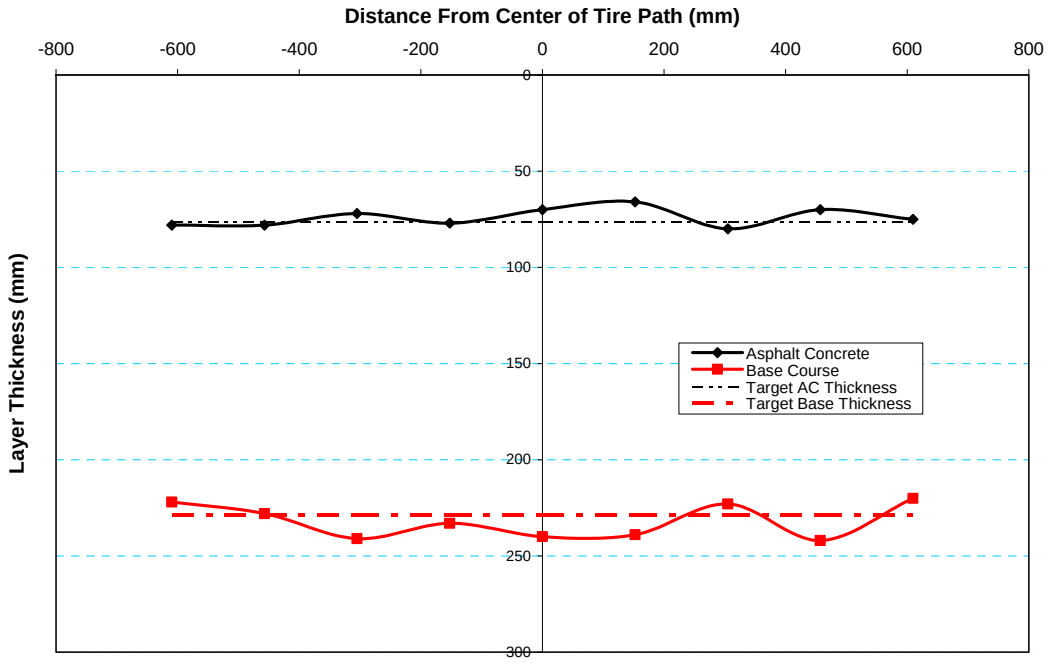

Figure 51. Layer thickness measurements across Test Window C2.

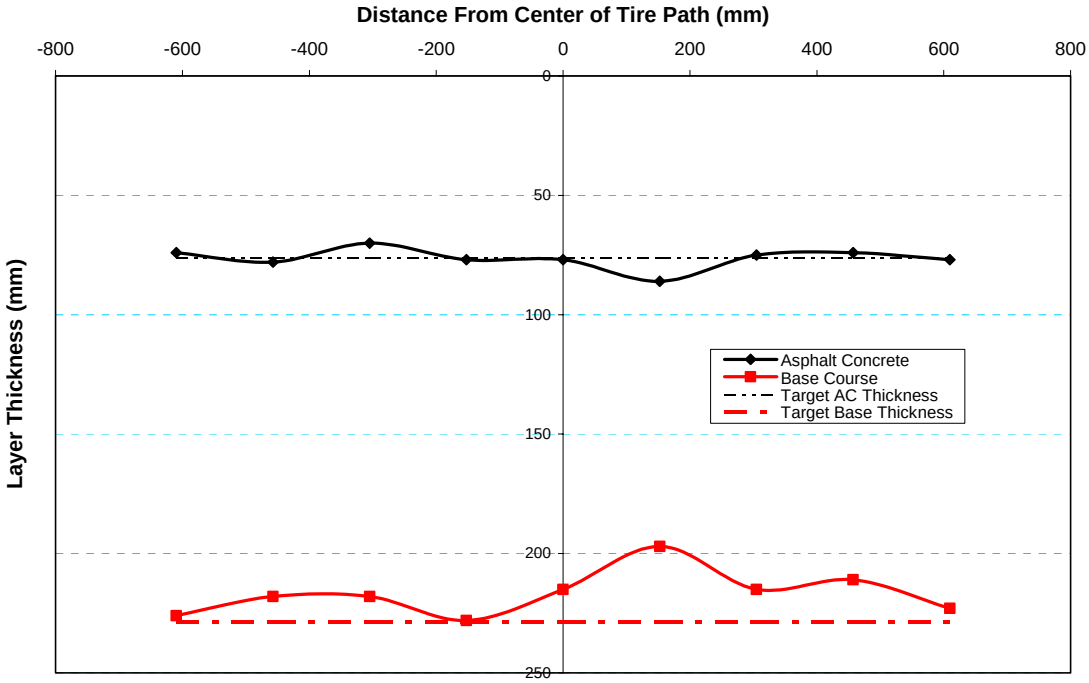

Figure 52. Layer thickness measurements across Test Window C3.

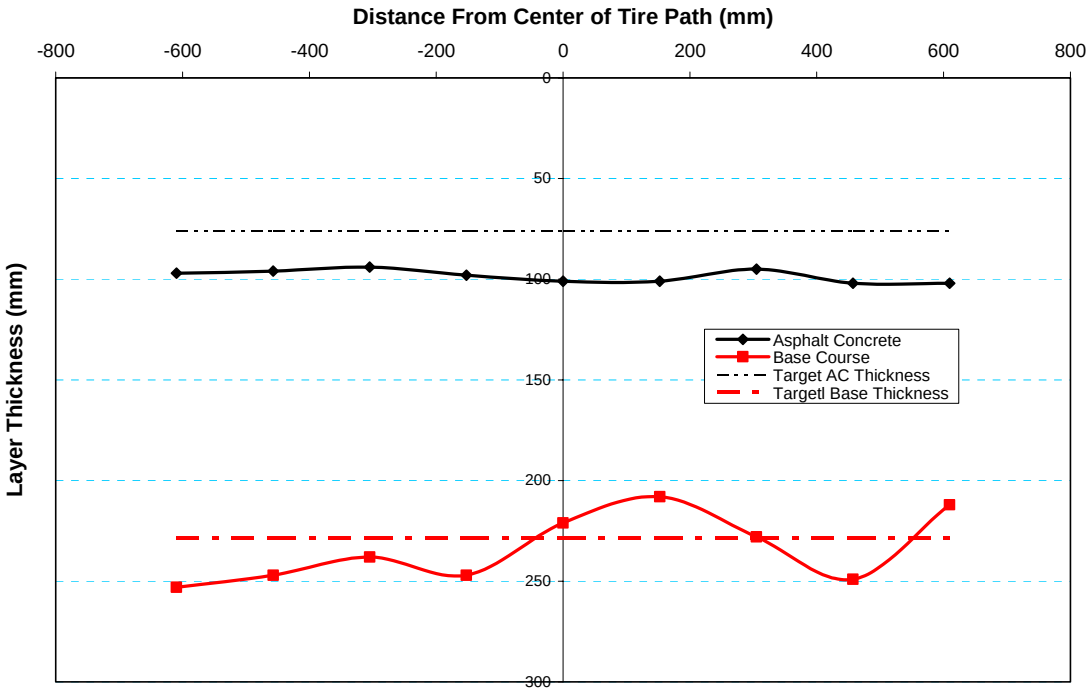

Figure 53. Layer thickness measurements across Test Window C4.

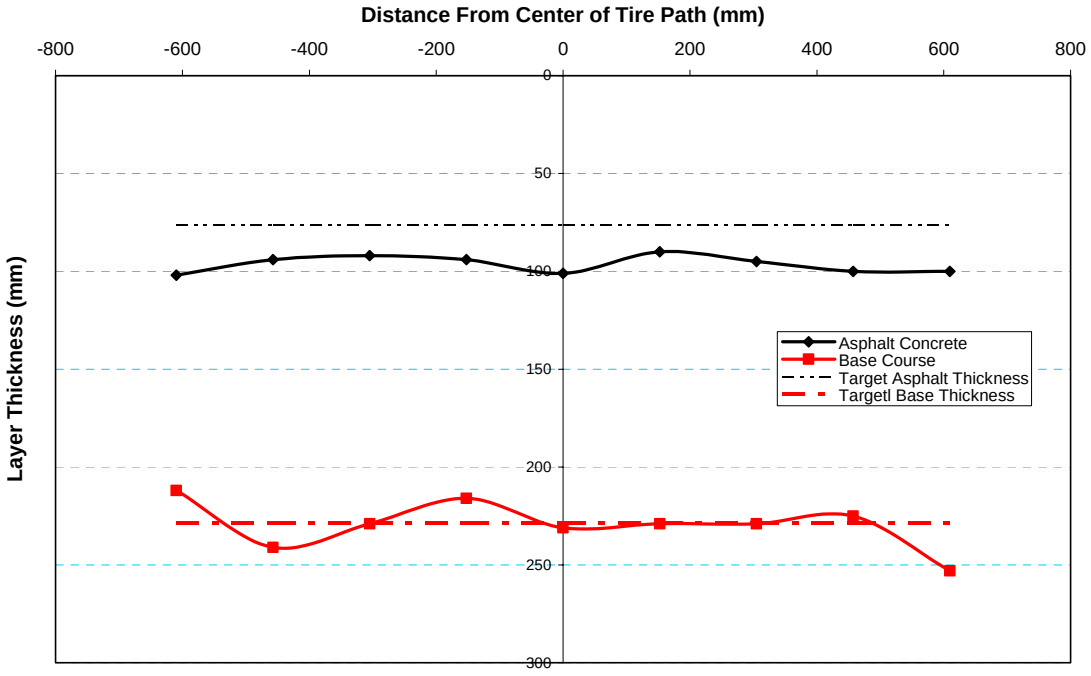

Figure 54. Layer thickness measurements across Test Window C5.

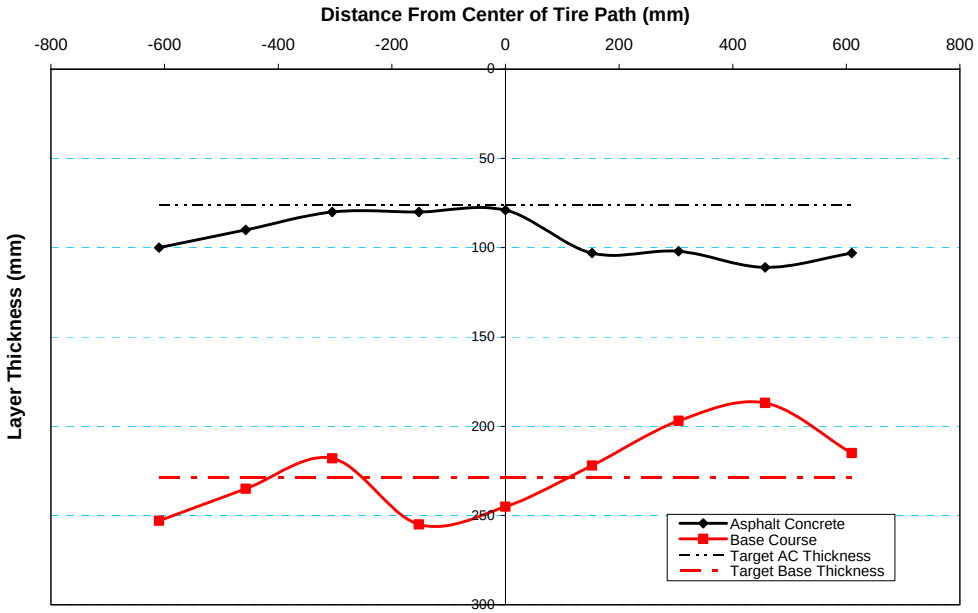

Figure 55. Layer thickness measurements across Test Window C6.

Dynamic cone penetrometer (DCP) measurements were conducted from the top of the subgrade down to a depth of at least 0.61 m (2 ft.). Figures 56 through 61 show profiles of CBR values obtained through DCP-CBR correlations. The average subgrade CBR value was 9 percent. According to Figure 19, this corresponds to a resilient modulus of 76 MPa (11,023 psi).

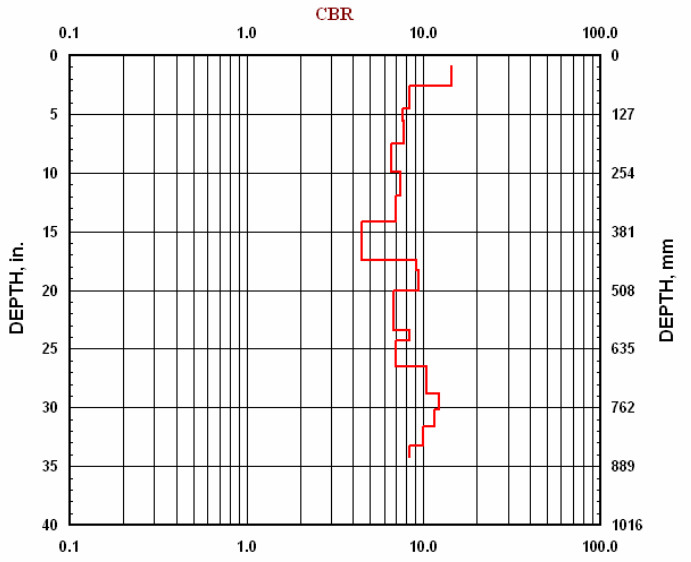

Figure 56. Subgrade CBR in Test Window C1.

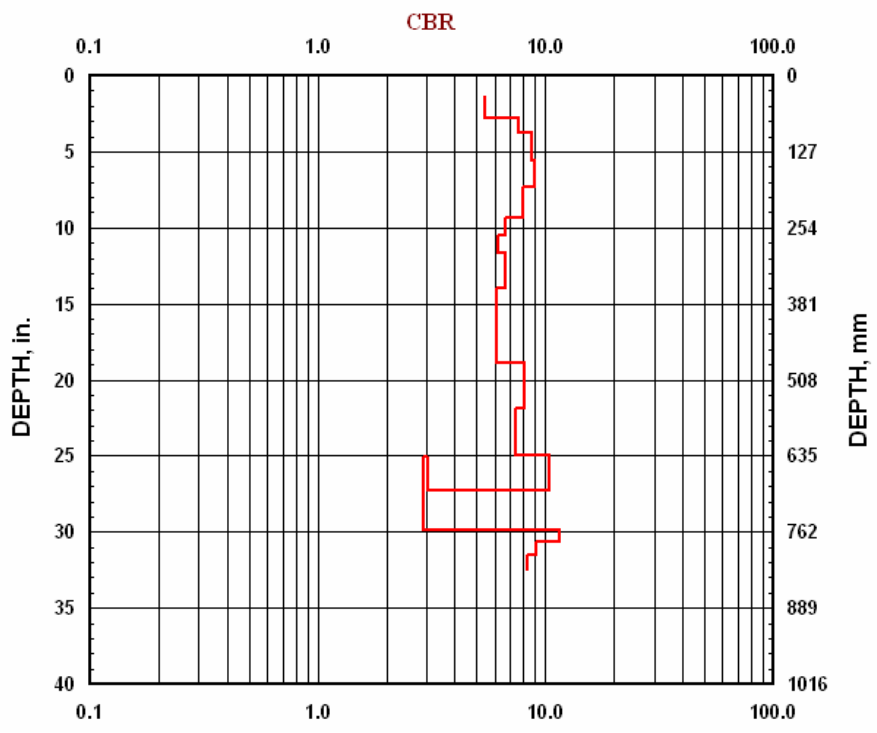

Figure 57. Subgrade CBR in Test Window C2.

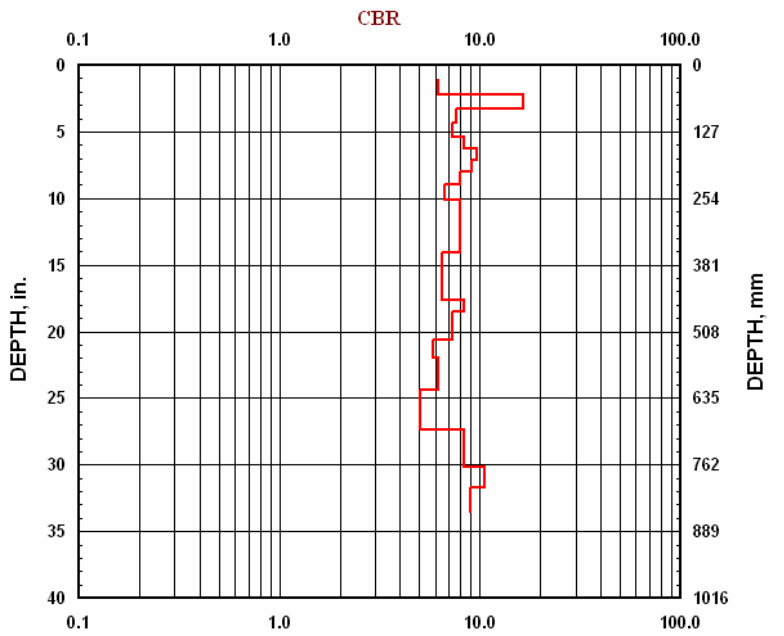

Figure 58. Subgrade CBR in Test Window C3.

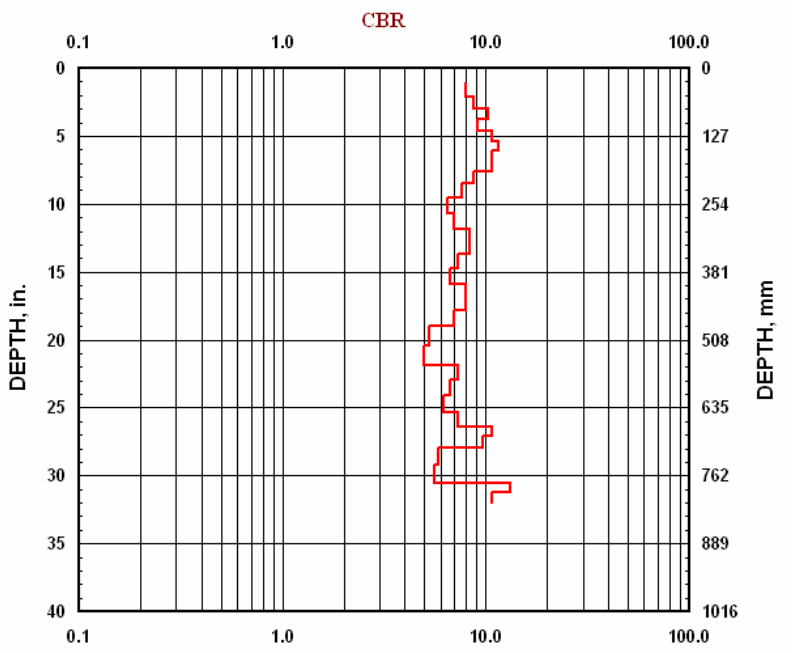

Figure 59. Subgrade CBR in Test Window C4.

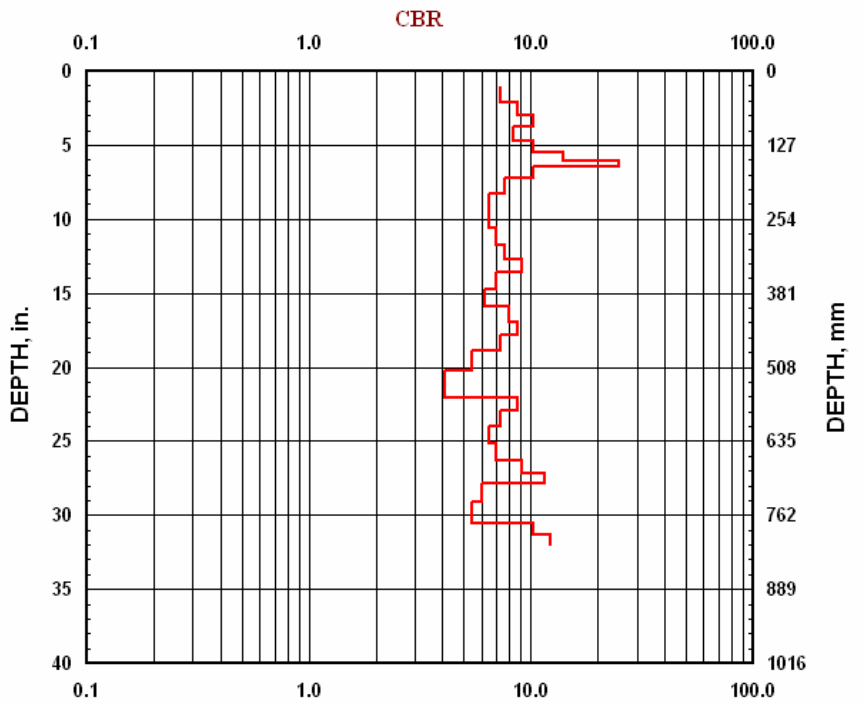

Figure 60. Subgrade CBR in Test Window C5.

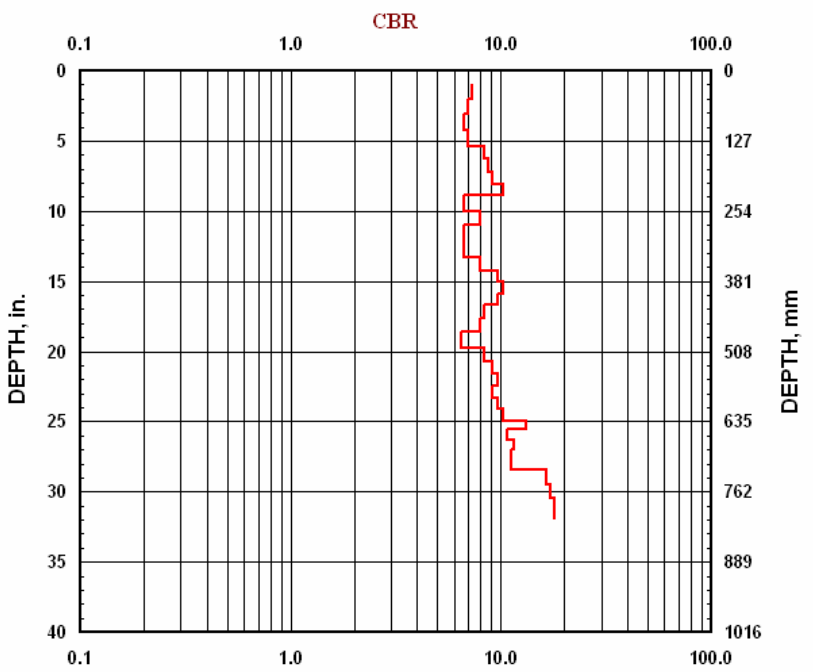

Figure 61. Subgrade CBR in Test Window C6.

SUMMARY AND CONCLUSIONS

Accelerated pavement testing (APT) was conducted on a test section with a subgrade soil that was classified as AASHTO type A-7-5 (USCS type ML). Hydrometer analysis indicated that 33 percent by weight of soil particles were in the range of clay particles. It appears that this clay content is sufficient for it to govern the bulk mechanical behavior of the subgrade soil. According to the experimental design, this test section was designed with a subgrade soil at moisture content higher than the optimum moisture content for this soil as determined by the modified Proctor method. The intended subgrade gravimetric content was 26 percent. The as-built subgrade soil moisture content was 25 percent. The subgrade was built in discrete layers 150-mm (6-in.) thick. Each soil layer was first spread to proper thickness while the soil was dryer than the target moisture content. The soil was then roto-tilled and moistened to meet the moisture specification. During this process, there were occasions when, at some locations, the bulk moisture content was approximately on target, but the soil became very sticky, weak and unstable. A closer inspection of these locations indicated that, while the bulk moisture content was correct, there were soil clumps where the localized moisture content at the clump surface was high while the center of the clump was drier. Because of the very low hydraulic conductivity of clay materials, zones of excessive moisture can coexist with zones of lower moisture content, and the higher moisture zones govern the behavior of the soil mass. Similar experience was obtained in a test section for a previous study (Perkins and Cortez, 2005).

As shown in Figure 20, approximately 25 million ESALs were needed to fail this test section. Considering the thin asphalt concrete in the pavement structure, this indicates a relatively strong subgrade. The number of ESALs needed to fail Test Section 712 (the control test section with subgrade soil at optimum moisture content) was 60 million. Although the pavement life was reduced in Test Section 711 due to the higher subgrade moisture content, both test sections were relatively strong compared to test sections built with other soils. However, with this AASHTO A-7-5 soil, if excessive moisture is allowed to enter the subgrade, the soil looses strength rapidly. When building roads over this subgrade soil type, special care must be exercised to provide drainage that reduces exposure to bulk water for significant periods of time. Concerns on the dry side are limited to shrinking cracking that can be dissipated by a granular sub-base, a drainage layer or the base course. Due to the very low hydraulic conductivity of soils with high clay content, they tend to have an equilibrium moisture content that depends on the long-term mean relative humidity of the geographic location.

Figure 40 shows again that the conventional criteria based on the resilient strain at the top of the subgrade at failure does not work well with all subgrade soils, and that soil type and moisture content must be considered. Similarly, performance prediction models must also be tailored separately to each soil type with moisture effects included.

REFERENCE

Dai, S.T., D.Van Deusen, D.Rettner and G.Cochran. "Investigation of Flexible Pavement Response to Truck Speed and FWD Load Through Instrumented Pavements", Proceedings of the 8th International Conference on Flexible Pavements. Seattle, Washington, pp.141-160. 1997.

Hilderbrand & Irwin, “Theoretical Analysis of Pavement Test Sections in the FERF”, Internal Report, 1994.

Janoo, V., L. Irwin, R. Eaton, and R. Haehnel, “Pavement Subgrade Performance Study: Project Overview, ERDC Report TR15, 2002.

1. Janoo, V., Irwin, L., and Haehnel, R. (2003) *Pavement Subgrade Performance Study Project Overview*, US Army Corps of Engineers. Engineer Research and Development Center. ERDC/ITL TR-03-5 March 2003.

APPENDIX A

SURFACE PROFILE TEST RESULTS

Table A1. Surface rut measurements in 711c1

Pass Number										
Cross Section	0	250	1,000	5,000	10,000	25,000	50,000	100,000	250,000	500,000
1	0	0.4	0.5	1.4	0.2	0.4	0.9	1.3	2.3	2.3
2	0	0.8	0.5	0.8	0.7	0.7	0.7	1.6	2.3	2.2
3	0	1.8	1.6	1.8	0.8	0.9	1.0	2.1	3.1	2.5
4	0	0.6	0.5	0.6	0.4	0.4	0.9	1.4	2.4	2.3
5	0	0.8	0.6	1.0	0.8	0.5	1.0	1.5	1.2	2.6
6	0	0.5	0.3	0.6	0.4	0.4	0.4	1.6	2.2	1.8
7	0	0.3	0.2	0.5	0.2	0.3	0.4	1.5	2.2	2.2
8	0	0.6	0.4	0.7	0.3	0.8	1.1	1.5	2.3	2.2
9	0	1.6	1.2	1.5	1.5	1.6	2.0	3.0	4.0	3.6
10	0	0.6	0.4	1.3	0.5	0.3	0.7	1.5	2.7	2.8
11	0	0.0	0.6	0.7	0.3	0.9	1.1	1.7	2.8	2.8
12	0	0.8	0.6	0.8	0.9	0.6	0.7	1.7	2.6	2.4
13	0	0.7	0.7	0.6	0.5	0.6	0.7	1.5	2.7	2.0
14	0	1.5	0.4	0.6	0.8	1.1	1.1	2.3	2.8	3.0
15	0	1.2	0.3	1.0	0.5	0.4	0.5	1.6	2.3	2.4
16	0	0.0	0.8	1.2	1.4	1.1	1.6	2.3	3.5	3.6
17	0	1.1	0.6	0.7	0.5	0.7	0.7	0.4	2.0	1.5
18	0	0.3	0.3	0.4	0.3	0.9	1.0	1.4	2.2	2.9
19	0	1.5	0.6	0.9	0.8	0.8	0.6	1.6	2.2	2.4
20	0	0.6	0.4	0.4	1.3	0.8	1.2	1.4	2.5	2.3

Table A 2. Surface rut measurements in 711C2

	Pass Number				
Cross Section	0	250	30,000	90,000	315,000
1	0	2.3	6.4	8.0	10.8
2	0	1.7	7.1	9.1	12.5
3	0	2.1	8.1	11.5	14.6
4	0	1.7	7.5	10.3	13.4
5	0	2.2	6.8	9.7	13.0
6	0	1.9	7.9	10.5	15.2
7	0	2.2	7.8	10.2	14.2
8	0	2.0	6.7	9.3	13.0
9	0	1.9	6.8	9.7	13.6
10	0	2.0	8.0	11.1	15.4
11	0	1.7	7.3	10.3	14.7
12	0	3.1	7.5	10.0	13.8
13	0	2.8	7.6	10.9	14.8
14	0	2.6	8.1	11.3	14.9
15	0	3.3	9.3	11.6	15.6
16	0	2.9	8.8	11.6	14.8
17	0	2.6	7.1	9.8	12.9
18	0	133.5	7.0	9.2	12.5
19	0	2.2	6.7	9.1	12.1
20	0	1.7	6.4	8.8	11.7

Table A 3. Surface rut measurements in 711C3

Pass Number								
Cross Section	0.1	250	1,000	5,000	10,000	25,000	100,000	200,000
1	0.1	1.2	2.2	2.7	3.2	3.8	5.5	6.3
2	0.1	1.3	2.0	2.8	3.7	4.4	5.9	6.8
3	0.1	1.3	2.2	3.2	3.8	4.3	5.7	6.6
4	0.1	1.3	1.6	2.5	2.8	3.5	5.4	6.2
5	0.1	1.3	1.9	2.6	3.0	3.7	5.3	6.4
6	0.1	1.4	2.0	2.9	3.6	4.5	6.4	7.1
7	0.1	1.3	2.0	2.9	3.4	4.4	5.9	6.9
8	0.1	1.4	2.3	3.3	4.2	5.0	5.9	7.5
9	0.1	1.2	1.9	2.7	3.5	4.3	6.3	7.0
10	0.1	1.7	2.4	2.8	3.2	4.0	6.1	6.6
11	0.1	1.0	1.4	2.5	2.9	4.1	6.0	6.7
12	0.1	1.2	1.3	3.1	3.4	3.8	5.0	6.1
13	0.1	1.2	1.3	2.7	3.5	3.6	5.2	6.2
14	0.1	1.6	1.9	3.4	3.7	4.3	5.6	6.5
15	0.1	1.8	2.0	3.0	3.3	4.3	5.4	6.5
16	0.1	1.4	2.1	2.5	3.3	3.8	5.0	5.8
17	0.1	1.2	1.8	2.4	2.5	3.2	4.5	5.4
18	0.1	1.1	1.3	2.4	2.9	3.4	4.5	5.3
19	0.1	1.1	1.4	2.1	2.7	3.8	4.7	5.3
20	0.1	1.9	2.2	2.8	3.4	3.8	5.3	5.5

Table A 4. Surface rut measurements in 711C4

Test Window	kips	kN
711C4	18	80

Cross Section	Traffic Passes				
Number	0	250	57,150	88,000	326,300
1	0	-0.8	-3.9	-4.7	6.0
2	0	-1.4	-4.2	-4.8	6.3
3	0	-1.2	-4.4	-5.0	6.5
4	0	-0.4	-3.7	-4.2	5.6
5	0	-0.7	-3.7	-4.2	5.8
6	0	-1.1	-3.8	-4.4	5.3
7	0	-1.2	-3.9	-4.7	5.7
8	0	-1.5	-4.4	-5.1	6.2
9	0	-1.2	-4.3	-4.7	5.8
10	0	-2.0	-4.6	-5.4	6.6
11	0	-1.7	-4.4	-5.2	6.1
12	0	-0.8	-4.1	-4.4	5.5
13	0	-1.2	-4.0	-4.5	5.8
14	0	-1.7	-3.8	-4.6	5.3
15	0	-1.6	-4.4	-4.3	5.8
16	0	-1.1	-3.9	-4.6	5.7
17	0	-1.0	-3.7	-3.9	5.2
18	0	-1.9	-3.4	-4.5	5.0
19	0	-1.6	4.0	-4.2	5.1
20	0	-1.3	-3.7	-3.9	5.6
Average	0	-1.3	-3.6	-4.6	5.7

Table A5. Surface rut measurements in 711C5

Semiaxial load = 40 kN											Semiaxial load = 80 kN		
Pass Number										0	60k	100k	250k
Cross Section	0	250	1k	5k	10k	25k	50k	100k	250k	500k	560k	600k	750k
1	0	0.9	0.8	1.6	2.3	2.1	2.6	3.3	4.0	5.7	7.9	6.5	7.4
2	0	0.7	1.2	1.6	2.3	2.7	2.6	3.6	4.2	5.2	7.4	6.9	7.2
3	0	1.6	1.5	1.8	2.2	2.3	2.5	3.6	4.5	4.9	6.6	6.4	7.2
4	0	0.7	1.0	1.7	1.9	2.3	2.7	3.3	4.3	5.3	6.8	7.2	7.7
5	0	0.7	0.6	1.3	1.5	2.2	2.2	3.4	3.9	4.9	6.6	6.6	7.5
6	0	1.0	1.1	2.1	2.4	2.7	3.1	4.4	5.1	5.5	7.0	7.8	8.2
7	0	0.4	0.7	1.3	1.3	2.0	2.0	3.1	4.2	4.4	5.7	6.3	6.6
8	0	0.8	0.8	1.6	1.6	2.1	2.2	3.5	3.8	5.2	6.2	6.6	7.3
9	0	1.4	1.0	1.6	1.9	2.5	2.4	3.5	4.5	5.5	6.6	6.8	7.2
10	0	0.8	1.2	1.3	2.0	1.8	2.4	3.1	4.7	5.6	6.5	7.2	7.9
11	0	0.8	1.0	1.3	1.7	0.9	2.7	3.5	4.3	5.8	6.9	6.8	7.7
12	0	0.7	0.9	1.4	1.8	2.2	2.2	3.5	4.5	5.3	6.5	7.5	7.3
13	0	0.5	0.8	1.1	1.7	1.7	2.1	3.1	4.2	4.9	6.0	6.2	7.0
14	0	0.8	0.7	1.5	1.9	2.0	2.2	3.1	4.4	5.1	6.2	6.5	6.8
15	0	0.7	0.9	0.9	1.4	1.5	1.8	2.7	3.6	4.7	5.7	6.0	6.7
16	0	1.4	1.0	1.3	2.0	2.4	2.5	3.6	4.5	5.3	6.2	6.9	7.4
17	0	1.0	1.0	1.6	2.0	2.0	2.9	3.2	4.2	5.0	6.0	6.2	6.7
18	0	1.0	0.9	1.1	1.5	2.1	2.0	3.2	4.3	5.1	6.3	6.8	7.2
19	0	0.6	0.9	1.3	1.8	2.0	2.4	2.9	4.2	4.7	6.1	6.6	7.2
20	0	0.9	1.1	1.5	1.8	2.1	2.4	3.2	4.4	4.9	6.5	6.9	7.8

Table A 6. Surface rut measurements in 711C6

	Pass Number				
Cross Section	0	250	1,000	81,400	205,550
1	0	2.7	3.6	12.9	18.9
2	0	1.7	2.8	13.5	27.1
3	0	2.3	3.3	14.6	26.0
4	0	2.4	3.4	14.2	27.0
5	0	1.9	2.7	13.3	24.1
6	0	2.0	2.6	13.3	19.0
7	0	1.0	2.1	10.5	17.7
8	0	1.9	2.4	10.9	17.5
9	0	1.5	2.7	11.2	15.5
10	0	1.9	2.7	11.2	15.3
11	0	2.3	3.0	12.0	18.5
12	0	2.2	3.4	11.9	16.4
13	0	2.1	2.6	10.8	15.2
14	0	1.6	2.8	10.5	14.9
15	0	1.8	2.4	9.8	13.3
16	0	1.2	2.6	8.9	11.7
17	0	1.4	2.2	8.1	10.8
18	0	1.4	2.0	7.9	10.7
19	0	1.8	2.3	8.3	10.8
20	0	1.4	2.1	7.4	10.1

APPENDIX B

PERMANENT DEFORMATION

AND

PERMANENT STRAIN

TEST RESULTS

Table B 1. Vertical permanent deformation (mm) in 711C1

Test Window	kips	kN
711C1	6	26.7

Layer	Depth	Traffic Passes									
	(mm)	0	250	1k	10k	25k	50k	100k	250k	480k	500k
AC	0-76	0	-0.05	-0.08	-0.21	-0.26	-0.31	-0.35	-0.46	-0.56	-0.61
Base-Top	76-190	0	-0.53	-0.57	-0.47	-0.39	-0.36	-0.33	-0.26	-0.34	-0.53
Base-Bottom	190-305	0	-0.31	-0.34	-0.35	-0.38	-0.38	-0.38	-0.38	-0.31	-0.42
Subgrade-Top	305-457	0	-0.24	-0.31	-0.31	-0.32	-0.31	-0.31	-0.32	-0.23	-0.35
Subgrade	457-610	0	-0.22	-0.29	-0.29	-0.31	-0.31	-0.33	-0.38	-0.38	-0.40
Subgrade	610-762	0	-0.11	-0.15	-0.14	-0.16	-0.16	-0.17	-0.19	-0.19	-0.20
Subgrade	762-914	0	-0.05	-0.07	-0.07	-0.08	-0.08	-0.08	-0.09	-0.09	-0.10
Subgrade	914-1067	0	-0.03	-0.04	-0.04	-0.04	-0.04	-0.04	-0.05	-0.05	-0.05
Subgrade	1067-1219	0	-0.01	-0.02	-0.02	-0.02	-0.02	-0.02	-0.02	-0.02	-0.02
Subgrade	1219-1372	0	-0.01	-0.01	-0.01	-0.01	-0.01	-0.01	-0.01	-0.01	-0.01
Subgrade	1372-1524	0	0.00	0.00	0.00	0.00	0.00	-0.01	-0.01	-0.01	-0.01
	Sum	0	-1.56	-1.88	-1.90	-1.97	-1.98	-2.02	-2.17	-2.18	-2.69

Table B 2. Vertical permanent deformation (mm) in 711C2

Test Window	kips	kN
711C2	22	97.9

Layer	Depth	Traffic Passes					
	(mm)	0	250	300,00	90,000	241,738	315,000
AC	0-76	0	-0.44	-3.78	-4.70	-5.10	-5.35
Base-Top	76-190	0	-0.37	-1.31	-1.96	-2.39	-2.46
Base-Bottom	190-305	0	-0.33	-0.57	-1.24	-1.82	-1.95
Subgrade-Top	305-457	0	-0.28	-0.58	-0.99	-1.01	-1.08
Subgrade	457-610	0	-0.50	-0.85	-1.58	-2.25	-2.34
Subgrade	610-762	0	-0.11	-0.06	-0.33	-0.21	-0.26
Subgrade	762-914	0	-0.06	-0.03	-0.17	-0.10	-0.13
Subgrade	914-1067	0	-0.03	-0.02	-0.08	-0.05	-0.06
Subgrade	1067-1219	0	-0.01	-0.01	-0.04	-0.03	-0.03
Subgrade	1219-1372	0	-0.01	0.00	-0.02	-0.01	-0.02
Subgrade	1372-1524	0	0.00	0.00	-0.01	-0.01	-0.01
	Sum	0	-2.14	-7.19	-11.13	-12.99	-13.70

Table B3. Vertical permanent deformation (mm) in 711C3

Test Window	kips	kN
711C3	18	80

Layer	Depth	Traffic Passes								
	(mm)	0	250	1k	5k	10k	25k	50k	100k	200k
AC	0-76	0	-0.12	-0.19	-0.60	-1.43	-2.13	-2.59	-3.15	-3.71
Base-Top	76-190	0	-0.23	-0.38	-0.44	-0.72	-0.93	-1.10	-1.25	-1.48
Base-Bottom	190-305	0	-0.11	-0.26	-0.23	-0.37	-0.48	-0.66	-0.74	-0.94
Subgrade-Top	305-457	0	0.04	-0.05	0.22	0.06	0.07	-0.09	-0.15	-0.37
Subgrade	457-610	0	0.06	0.00	0.17	-0.04	-0.02	-0.04	0.10	0.06
Subgrade	610-762	0	0.07	-0.07	0.08	0.00	-0.05	-0.06	0.07	0.08
Subgrade	762-914	0	0.12	0.13	0.32	0.08	0.19	0.18	0.36	0.43
Subgrade	914-1067	0	0.12	-0.35	-0.16	0.10	-0.29	-0.28	-0.15	-0.11
Subgrade	1067-1219	0	-0.15	-0.59	-0.40	0.49	-0.50	-0.49	-0.38	-0.35
Subgrade	1219-1372	0	-0.21	-0.19	0.14	-0.67	0.04	0.04	0.22	0.23
Subgrade	1372-1524	0	-0.26	-0.32	-0.08	-0.09	-0.24	-0.24	-0.12	-0.15
	Sum	0	-0.67	-2.27	-0.98	-2.59	-4.33	-5.32	-5.19	-6.30

Table B4. Vertical permanent deformation (mm) in 711C4

Test Window	kips	kN
711C4	18	80

Layer	Depth	Traffic Passes						
	(mm)	0	250	1,260	57,150	88,000	168,000	326,300
AC	0-76	0	-1.15	-1.70	-2.47	-2.79	-2.90	-3.11
Base-Top	76-190	0	-0.11	-0.35	-1.10	-0.89	-1.10	-1.48
Base-Bottom	190-305	0	-0.04	-0.25	-0.36	-0.24	-0.43	-0.96
Subgrade-Top	305-457	0	-0.02	-0.05	-0.09	-0.23	-0.28	-0.37
Subgrade	457-610	0	-0.06	0.01	-0.04	-0.16	-0.28	-0.18
Subgrade	610-762	0	-0.04	-0.07	-0.06	-0.23	-0.31	-0.11
Subgrade	762-914	0	-0.06	-0.13	-0.18	-0.28	-0.12	-0.43
Subgrade	914-1067	0	-0.18	-0.35	-0.28	-0.28	-0.23	-0.11
Subgrade	1067-1219	0	-0.29	-0.59	-0.49	-0.59	-0.39	-0.15
Subgrade	1219-1372	0	-0.10	-0.19	0.04	-0.08	-0.03	-0.23
Subgrade	1372-1524	0	-0.16	-0.32	-0.24	-0.20	-0.20	-0.15
	Sum	0	-2.20	-3.99	-5.27	-5.96	-6.27	-7.27

Table B5. Vertical permanent deformation (mm) in 711C5

	Test Window	Load in kips (kN)									Load in kips (kN)		
	711C5	9 (40)									18 (80)		
	Depth	Traffic Passes											
Layer	(mm)	0	250	1k	5k	10k	50k	100k	250k	500k	560k	600k	750k
AC	0-76	0	-1.01	-0.91	-1.11	-1.61	-1.99	-2.66	-3.31	-3.40	-3.68	-3.86	-4.22
Base-Top	76-190	0	-0.33	-0.15	-0.24	-0.46	-0.56	-0.74	-0.80	-0.88	-0.99	-1.09	-1.29
Base-Bottom	190-305	0	-0.27	-0.08	-0.13	-0.32	-0.39	-0.55	-0.58	-0.65	-0.86	-0.88	-0.93
Subgrade-Top	305-457	0	-0.33	-0.05	-0.09	-0.33	-0.37	-0.54	-0.64	-0.74	-0.79	-0.80	-0.75
Subgrade	457-610	0	-0.38	-0.05	-0.11	-0.37	-0.30	-0.44	-0.47	-0.46	-0.49	-0.51	-0.36
Subgrade	610-762	0	-0.30	0.00	-0.03	-0.25	-0.18	-0.29	-0.30	-0.22	-0.23	-0.24	-0.12
Subgrade	762-914	0	-0.15	0.00	-0.02	-0.13	-0.09	-0.15	-0.15	-0.11	-0.12	-0.12	-0.06
Subgrade	914-1067	0	-0.07	0.00	-0.01	-0.06	-0.05	-0.07	-0.07	-0.06	-0.06	-0.06	-0.03
Subgrade	1067-1219	0	-0.04	0.00	0.00	-0.03	-0.02	-0.04	-0.04	-0.03	-0.03	-0.03	-0.01
Subgrade	1219-1372	0	-0.02	0.00	0.00	-0.02	-0.01	-0.02	-0.02	-0.01	-0.01	-0.02	-0.01
Subgrade	1372-1524	0	-0.01	0.00	0.00	-0.01	-0.01	-0.01	-0.01	-0.01	-0.01	-0.01	0.00
	Sum	0	-2.91	-1.25	-1.75	-3.58	-3.97	-5.51	-6.39	-6.58	-7.27	-7.62	-7.78

Table B6. Vertical permanent deformation (mm) in 711C6

	Test Window	kips	kN			
	711C6	22	97.9			
Layer	Depth	Traffic Passes				
	(mm)	0	250	1,000	82,400	205,550
AC	0-76	0	0.35	1.50	3.79	3.79
Base-Top	76-190	0	0.89	0.85	3.30	4.12
Base-Bottom	190-305	0	0.09	0.22	1.14	1.66
Subgrade-Top	305-457	0	0.08	0.28	1.50	2.24
Subgrade	457-610	0	0.07	0.33	2.85	4.38
Subgrade	610-762	0	0.08	0.26	1.06	1.43
Subgrade	762-914	0	0.04	0.13	0.53	0.71
Subgrade	914-1067	0	0.02	0.06	0.26	0.36
Subgrade	1067-1219	0	0.01	0.03	0.13	0.18
Subgrade	1219-1372	0	0.01	0.02	0.07	0.09
Subgrade	1372-1524	0	0.00	0.01	0.03	0.04
	Sum	0	1.63	3.68	14.67	19.00

Table B7. Permanent strains in 711C1

Test Window	kips	kN
711C1	6	26.7

Depth	Traffic Passes									
(mm)	0	250	1,000	5,000	25,000	50,000	100,000	250,000	480,100	500,000
49	0	-675	-1,012	-2,021	-3,359	-4,025	-4,557	-6,013	-7,330	-7,986
155	0	-4,621	-4,957	-4,464	-3,350	-3,154	-2,835	-2,231	-2,917	-4,605
269	0	-2,704	-2,970	-2,872	-3,296	-3,299	-3,269	-3,316	-2,661	-3,670
396	0	-2,052	-2,717	-2,599	-2,800	-2,693	-2,664	-2,781	-2,026	-3,013
543	0	-1,899	-2,532	-2,353	-2,737	-2,733	-2,907	-3,303	-3,279	-3,440
695	0	-950	-1,266	-1,177	-1,369	-1,366	-1,454	-1,651	-1,639	-1,720
847	0	-475	-633	-588	-684	-683	-727	-826	-820	-860
1000	0	-237	-317	-294	-342	-342	-363	-413	-410	-430
1152	0	-119	-158	-147	-171	-171	-182	-206	-205	-215
1305	0	-59	-79	-74	-86	-85	-91	-103	-102	-107
1457	0	-30	-40	-37	-43	-43	-45	-52	-51	-54

Table B8. Permanent strains in 711C2

	Test Window	kips	kN
	711C2	22	97.9

Layer	Depth	Traffic Passes					
	(mm)	0	250	30,000	90,000	241,738	315,000
AC	38	0	-4,453	-38,543	-48,005	-51,997	-54,638
Base-Top	133	0	-3,230	-11,428	-17,145	-20,910	-21,550
Base-Bottom	248	0	-2,889	-4,947	-10,867	-15,947	-17,087
Subgrade-Top	381	0	-2,014	-4,125	-7,084	-7,250	-7,730
Subgrade	533	0	-3,268	-5,570	-10,391	-14,779	-15,382
Subgrade	686	0	-751	-402	-2,178	-1,377	-1,684
Subgrade	838	0	-376	-201	-1,089	-689	-842
Subgrade	991	0	-188	-101	-544	-344	-421
Subgrade	1143	0	-94	-50	-272	-172	-210
Subgrade	1295	0	-47	-25	-136	-86	-105
Subgrade	1448	0	-23	-13	-68	-43	-53

Table B9. Permanent strains in 711C3

Test Window	kips	kN
711C3	18	80

Layer	Depth	Traffic Passes								
	(mm)	0	250	1,000	5,000	10,000	25,000	50,000	100,000	200,000
AC	49	0	-1,231	-1,968	-6,124	-14,569	-21,691	-26,381	-32,179	-37,907
Base-Top	155	0	-1,978	-3,292	-3,871	-6,302	-8,085	-9,602	-10,942	-12,891
Base-Bottom	269	0	-811	-1,886	-1,640	-2,619	-3,408	-4,748	-5,313	-6,762
Subgrade-Top	396	0	292	-342	1,423	366	440	-593	-966	-2,409
Subgrade	543	0	417	2	1,131	-286	-113	-232	673	426
Subgrade	695	0	439	-429	529	11	-306	-395	481	532
Subgrade	847	0	765	851	2,096	558	1,268	1,195	2,392	2,820
Subgrade	1000	0	771	-2,298	-1,052	632	-1,930	-1,810	-992	-706
Subgrade	1152	0	-983	-3,854	-2,615	3,204	-3,282	-3,193	-2,493	-2,266
Subgrade	1305	0	-1,396	-1,249	925	-4,376	234	270	1,435	1,510
Subgrade	1457	0	-1,687	-2,123	-533	-577	-1,602	-1,606	-778	-985

Table B10. Permanent strains in 711C4

Test Window	kips	kN
711C4	18	80

Layer	Depth	Traffic Passes						
	(mm)	0	250	1,260	57,150	88,000	168,000	326,300
AC	49	0	-11,782	-17,527	-25,413	-28,738	-29,840	-32,032
Base-Top	155	0	-765	-2,365	-7,495	-6,034	-7,507	-10,061
Base-Bottom	269	0	-270	-1,730	-2,470	-1,652	-2,940	-6,515
Subgrade-Top	396	0	-131	-356	-616	-1,584	-1,906	-2,503
Subgrade	543	0	-391	71	-241	-1,066	-1,911	-1,260
Subgrade	695	0	-271	-446	-411	-1,597	-2,115	-757
Subgrade	847	0	-442	-884	-1,241	-1,923	-841	-2,929

Table B11. Permanent strains in 711C5

	Test Window	Load in kips (kN)									
	711C5	9 (40)							18 (80)		
Layer	Depth	Traffic Passes									
	(mm)	0	250	1,000	5,000	25,000	100,000	500,000	560,000	600,000	750,000
AC	49	0	-10,342	-9,324	-11,357	-16,382	-27,150	-34,743	-37,542	-39,392	-43,059
Base-Top	155	0	-2,858	-1,340	-2,063	-2,349	-6,495	-7,741	-8,661	-9,536	-11,286
Base-Bottom	269	0	-2,370	-698	-1,118	-997	-4,778	-5,652	-7,524	-7,699	-8,136
Subgrade-Top	396	0	-2,361	-335	-671	-275	-3,884	-5,316	-5,648	-5,736	-5,360
Subgrade	543	0	-2,464	-351	-729	386	-2,893	-3,041	-3,217	-3,333	-2,389
Subgrade	695	0	-1,967	-17	-226	783	-1,926	-1,467	-1,523	-1,594	-766
Subgrade	847	0	-983	-8	-113	391	-963	-733	-761	-797	-383
Subgrade	1000	0	-492	-4	-57	196	-482	-367	-381	-399	-191
Subgrade	1152	0	-246	-2	-28	98	-241	-183	-190	-199	-96
Subgrade	1305	0	-123	-1	-14	49	-120	-92	-95	-100	-48
Subgrade	1457	0	-61	-1	-7	24	-60	-46	-48	-50	-24

Table B12. Permanent strains in 711C6

	Test Window	kips	kN
	711C6	22	97.9

Layer	Depth	Traffic Passes				
	(mm)	0	250	1,000	82,400	205,550
AC	49	0	3,587	15,291	38,674	38,674
Base-Top	155	0	7,783	7,398	21,756	36,024
Base-Bottom	269	0	750	1,941	10,012	14,512
Subgrade-Top	396	0	544	1,983	10,771	16,006
Subgrade	543	0	440	2,136	18,708	28,765
Subgrade	695	0	535	1,706	6,925	9,378
Subgrade	847	0	267	853	3,462	4,689
Subgrade	1000	0	134	426	1,731	2,345
Subgrade	1152	0	67	213	866	1,172
Subgrade	1305	0	33	107	433	586
Subgrade	1457	0	17	53	216	293

APPENDIX C

RESILIENT STRAIN

TEST RESULTS

Table C 1. Resilient vertical strain (microstrains) in base and subgrade in TS711C1.

Test Window	kips	kN
711C1	6	26.7

Layer	Depth	Traffic Passes								
	(mm)	0	250	1,000	5,000	10,000	50,000	100,000	480,100	500,000
Base-Top	155	-1,115	-1,279	-1,154	-1,390	-1,429	-1,670	-1,410	-1,410	-1,288
Base-Bottom	269	-176	-239	-243	-284	-266	-279	-245	-227	-184
Subgrade-Top	396	-379	-500	-423	-536	-443	-464	-458	-444	-407
Subgrade	543	-200	-322	-259	-293	-278	-276	-282	-260	-241
Subgrade	695	-254	-318	-257	-293	-273	-269	-276	-261	-253
Subgrade	847	-152	-231	-189	-208	-195	-245	-161	-171	-209
Subgrade	1000	-82	-97	-86	-101	-88	-83	-95	-70	-67
Subgrade	1152	-189	-267	-242	-245	-181	-215	-246	-211	-188
Subgrade	1305	-18	-11	-21	-6	-2	-19	3	11	7
Subgrade	1457	40	33	45	38	38	41	44	52	59

Table C 2. Resilient vertical strain (microstrains) in base and subgrade in TS711C2.

Test Window	kips	kN
711C2	22	97.9

Layer	Depth	Traffic Passes				
	(mm)	0	250	30,000	90,000	315,000
Base-Top	155	-3,740	-4,349	-5,926	-6,819	-6,338
Base-Bottom	269	-2,282	-2,954	-5,961	-8,074	-7,523
Subgrade-Top	396	-1,545	-1,946	-3,034	-3,740	-4,504
Subgrade	543	-1,510	-1,993	-3,159	-4,068	-4,472
Subgrade	695	-894	-1,004	-1,593	-2,013	-2,075
Subgrade	847	-723	-858	-1,188	-1,435	-1,477
Subgrade	1000	-393	-494	-572	-634	-700
Subgrade	1152	-266	-265	-315	-342	-360
Subgrade	1305	-175	-196	-238	-278	-281
Subgrade	1457	-82	-11	-141	-173	-164

Table C 3. Resilient vertical strain (microstrains) in base and subgrade in TS711C3.

Test Window	kips	kN
711C3	18	80

Layer	Depth	Traffic Passes								
	(mm)	0.1	250	1,000	5,000	10,000	25,000	50,000	100,000	200,000
Base-Top	155	-4,298	-5,010	-5,397	-5,735	-5,897	-6,020	-6,557	-6,700	-6,715
Base-Bottom	269	-2,178	-2,524	-2,796	-3,193	-3,516	-3,672	-4,506	-4,684	-4,923
Subgrade-Top	396	-1,193	-1,480	-1,704	-1,904	-2,014	-2,331	-2,823	-2,858	-3,014
Subgrade	543	-759	-943	-1,096	-1,204	-1,285	-1,348	-1,636	-1,709	-2,009
Subgrade	695	-859	-1,015	-1,113	-1,260	-1,294	-1,356	-1,648	-1,677	-1,828
Subgrade	847	-346	-407	-449	-495	-512	-547	-623	-630	-701
Subgrade	1000	-159	-197	-211	-238	-230	-251	-289	-283	-318
Subgrade	1152	-173	-183	-190	-212	-218	-209	-251	-253	-255
Subgrade	1305	-176	-202	-144	-168	-233	-213	-218	-219	-195
Subgrade	1457	-45	33	-123	-71	-75	-89	-28	-129	-93

Table C 4. Resilient vertical strain (microstrains) in base and subgrade in TS711C4.

Test Window	kips	kN
711C4	18	80

Layer	Depth	Traffic Passes						
	(mm)	0	250	1,260	57,150	88,000	168,000	326,300
Base-Top	155	0	GF	GF	GF	GF	GF	GF
Base-Bottom	269	0	GF	GF	GF	GF	GF	GF
Subgrade-Top	396	0	-1,291	-1,447	-1,616	-2,506	-2,236	-2,449
Subgrade	543	0	-1,135	-1,286	-1,457	-2,108	-1,999	-2,106
Subgrade	695	0	-721	-779	-882	-1,211	-1,200	-1,136
Subgrade	847	0	-971	-1,039	-1,134	-1,466	-1,454	-1,348
Subgrade	847	0	10	9	10	12	16	8
Subgrade	1000	0	6	15	22	12	3	17
Subgrade	1152	0	-147	-142	-147	-189	-198	-110
Subgrade	1305	0	-58	-57	-64	-85	-83	-79

Table C 5. Resilient vertical strain (microstrains) in base and subgrade in TS711C5.

	Test Window	Load in kips (kN)									
	711C5	9 (40)							18 (80)		
Layer	Depth	Traffic Passes									
	(mm)	0	250	1,000	5,000	25,000	100,000	500,000	560,000	600,000	750,000
Base-Top	155	-2,875	-2,545	-2,606	-2,893	-2,864	-3,121	-2,722	-3,602	-3,537	-3,625
Base-Bottom	269	-1,057	-1,067	-1,042	-1,199	-1,138	-1,545	-1,154	-2,732	-2,602	-2,799
Subgrade-Top	396	-399	-427	-404	-502	-516	-756	-540	-2,103	-2,179	-2,402
Subgrade	543	-363	-338	-362	-384	-409	-551	-412	-1,329	-1,248	-1,420
Subgrade	695	-305	-277	-285	-279	-341	-392	-319	-970	-987	-1,007
Subgrade	847	-243	-274	-273	-296	-278	-348	-299	-646	-672	-666
Subgrade	1000	58	64	86	60	62	101	99	94	86	67
Subgrade	1152	29	14	27	20	24	25	21	5	23	14
Subgrade	1305	30	24	31	26	25	14	16	7	-5	-9
Subgrade	1457	137	145	167	137	141	141	137	138	132	139

Table C 6. Resilient vertical strain (microstrains) in base and subgrade in TS711C6.

	Test Window	kips	kN			
	711C6	22	97.9			
Layer	Depth	Traffic Passes				
	(mm)	0	250	1,000	82,400	205,550
Base-Top	155	-3,907	-10,350	-13,507	-15,536	-15,625
Base-Bottom	269	-3,554	-4,219	-4,757	-10,846	-13,199
Subgrade-Top	396	-1,766	-2,286	-2,735	-6,025	-7,017
Subgrade	543	-1,179	-1,537	-1,834	-4,008	-4,639
Subgrade	695	-1,164	-1,399	-1,578	-3,135	-3,690
Subgrade	847	-11	-9	-8	-45	-86
Subgrade	1000	82	81	78	57	-1
Subgrade	1152	11	39	24	23	36
Subgrade	1305	-214	-210	-291	-304	-325
Subgrade	1457	66	-1	3	-31	-45

Table C 6. Resilient vertical strain (microstrains) in base and subgrade in TS711C6.

	Test Window	kips	kN			
	711C6	22	97.9			
Layer	Depth	Traffic Passes				
	(mm)	0	-277	-285	-279	-334.1953
Base-Top		-3,907	-10,350	-13,507	-23,622	-33,123
Base-Bottom		-3,554	-4,219	-4,757	-10,846	-13,199
Subgrade-Top		-1,766	-2,286	-2,735	-6,025	-7,017
Subgrade		-1,179	-1,537	-1,834	-4,008	-4,639
Subgrade		-1,164	-1,399	-1,578	-3,135	-3,690

APPENDIX D

STRESS MEASUREMENTS

Table D 2. Stress (kPa) 76 mm below base-subgrade interface in TS711C1.

Test Window	kips	kN							
711C1	6	27							
Depth	Traffic Passes								
(mm)	0.1	250	1,000	5,000	25,000	50,000	100,000	250,000	480,100	500,000
381	36.2	45.4	36.4	49.4	40.8	39.7	40.5	50.6	49.6	47.3

Table D 2. Stress (kPa) in base and subgrade in TS711C2.

	Test Window	kips	kN			
	711C2	22	97.9			
	Depth		Traffic Passes			
	(mm)	0	250	30,000	90,000	315,000
Middle of base	191	239.9	256.2	240.8	236.3	247.1
76 mm below top of subgrade	381	No sensor				
381 mm below top of subgrade	686	17.9	20	20.5	24	24

Table D 3. Stress (kPa) 76 mm below base-subgrade interface in TS711C3.

Test Window	kips	kN							
711C3	18	80							
Depth	Traffic Passes								
(mm)	0	250	1,000	5,000	10,000	25,000	50,000	100,000	200,000
381	121.9	128.1	133.6	128.4	129.4	126.0	124.4	104.9	107.4

Table D 4. Stress (kPa) 76 mm below base-subgrade interface in TS711C4.

Test Window	kips	kN					
711C4	18	80					
Depth	Traffic Passes						
(mm)	0	250	1,260	57,150	88,000	168,000	326300
381	128.4	124.8	130.4	128.2	116.6	112.8	112.2

Table D 5. Stress (kPa) 76 mm below base-subgrade interface in TS711C5.

Test Window	kips	kN						kips	kN	
711C5	9	40						18	80	
Depth	Traffic Passes									
(mm)	0	250	1,000	5,000	25,000	100,000	500,000	560,000	600,000	750,000
381	22.1	22.1	21.8	20.1	20.9	26.1	22.1	38.9	35	30.3

Table D 6. Stress (kPa) in base and subgrade TS711C6.

Test Window	kips	kN			
711C6	22	97.9			
Depth	Traffic Passes				
(mm)	0	250	1,000	82,400	205,550
Top of Base Course	90	111.9	123.1	130.4	172.4	172.2
Bottom of Base Course	292	233.7	243.5	246.2	225	215.7
76 mm below top of subgrade	381	98.7	97	97.3	192	232.2

APPENDIX E

FALLING WEIGHT DEFLECTOMETER

MEASUREMENTS

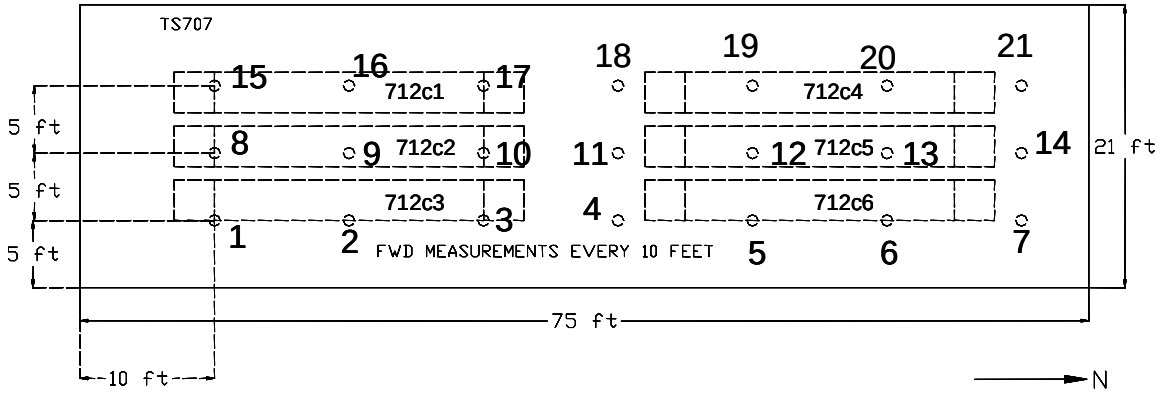

Figure E1. Location of FWD tests in Test Section 711.

Table F 1. FWD tests at 21 locations in Test Section 711.

		Sensor Radial Distance (in)						
		0	12	24	36	48	60	72
Station #	Load (lb)	W1	W2	W3	W4	W5	W6	W7
1	7,826	24.89	10.79	4.08	2.59	1.44	1.81	1.48
2	7,702	26.92	10.52	3.76	2.51	1.97	1.52	1.24
3	7,510	26.68	10.59	3.78	2.45	1.89	1.48	1.17
4	7,442	29.03	12.43	4.18	2.68	1.44	1.39	1.25
5	7,442	27.93	10.46	3.77	2.45	1.85	1.44	1.16
6	7,464	20.12	8.7	3.85	2.53	1.89	1.46	1.16
7	7,408	19.23	8.68	4.02	2.55	1.82	1.36	1.06
8	7,555	26.76	12.73	3.74	2.93	1.6	1.54	1.33
9	7,374	28.25	11.5	3.89	2.25	1.69	1.39	1.12
10	7,442	24.27	9.97	3.88	2.48	1.87	1.5	1.22
11	7,385	19.93	9.6	4.09	2.57	1.95	1.55	1.26
12	7,476	16.94	8.25	3.83	2.5	1.92	1.5	1.19
13	7,283	18.85	8.36	3.8	2.58	1.99	1.57	1.28
14	7,374	18.83	8.54	3.91	2.54	1.93	1.46	1.14
15	7,894	33.49	11.02	4.17	2.65	1.83	1.39	1.07
16	7,170	25.2	10.56	3.98	2.28	1.65	1.28	1.02
17	7,148	21.53	9.79	3.51	2.33	1.73	1.37	1.09
18	7,182	20.95	9.91	3.98	2.38	1.78	1.37	1.09
19	7,114	16.02	8.09	3.83	2.41	1.77	1.35	1.05
20	7,069	20.28	9.49	3.89	2.41	1.78	1.36	1.05
21	7,012	23.61	8.84	3.71	2.41	1.73	1.3	0.99

Test Section 711 AASHTO A-7-5 subgrade soil at 25 percent moisture content (Optimum moisture is 20.5 percent)